Following nuclei through nucleosynthesis: A novel tracing technique

T. M. Sprouse [1,2,3] M. R. Mumpower [2,3] and R. Surman [1]

[1]*Department of Physics, University of Notre Dame, Notre Dame, Indiana 46556, USA*
[2]*Theoretical Division, Los Alamos National Laboratory, Los Alamos, New Mexico 87545, USA*
[3]*Center for Theoretical Astrophysics, Los Alamos National Laboratory, Los Alamos, New Mexico 87545, USA*

Astrophysical nucleosynthesis is a family of diverse processes by which atomic nuclei undergo nuclear reactions and decay to form new nuclei. The complex nature of nucleosynthesis, which can involve as many as tens of thousands of interactions between thousands of nuclei, makes it difficult to study any one of these interactions in isolation using standard approaches. In this work, we present a new technique, nucleosynthesis tracing, that we use to quantify the relative fraction of nuclear abundances that pass through individual nuclear reaction, decay, and fission processes at any point during nucleosynthesis. We apply this technique to study fission and β^- decay as they occur in the rapid neutron capture (r) process of nucleosynthesis.

I. INTRODUCTION

The extreme conditions that can arise in astrophysical environments enable nuclear transmutation processes to take place, by which atomic nuclei interact with their environment or decay to form new nuclei. Insofar as different astrophysical environments may foster certain transmutation processes but not others, these environments may be categorized by the different types of nucleosynthesis that occur in each; one of the primary goals of nuclear astrophysics, then, is to explain how these different nucleosynthesis sources produce all of the chemical elements observed in the universe, beginning with the primordial hydrogen and helium produced during the Big Bang [1].

In the most complex cases, nucleosynthesis can involve many thousands of nuclear species connected by upward of ≈100 000 nuclear transmutation processes by which their abundances may evolve in time. Because the rates at which the different processes occur may depend on the temperature and density of the environment in which the nuclei are situated, as well as the abundances of the different nuclei themselves, nucleosynthesis is an extremely dynamical and nonlinear problem. Nevertheless, through the use of nuclear reaction networks, it is possible to effectively model nucleosynthesis numerically.

More difficult, however, is the problem of isolating and quantifying the role of individual nuclear properties as they influence nucleosynthesis as a whole. This can be especially important because nucleosynthesis is inherently determined by the properties of the nuclei that participate in it, making these properties the focus of a significant number of experimental and theoretical campaigns in nuclear physics (see, e.g., Refs. [2–7] and references therein). By identifying the most crucial nuclear properties for each nucleosynthesis process, these campaigns may be more precisely focused in the near future on those properties which will most significantly constrain nucleosynthesis simulation predictions.

Past approaches to accomplish this goal have either (1) systematically varied individual or collections of nuclear properties and examined the relative changes to nucleosynthesis, for example, in Refs. [8–15], or (2) analyzed the overall rate at which different processes (reactions, decays, or fission) occur during nucleosynthesis, such as in Refs. [16–18]. However, it has not been possible using current techniques to precisely quantify which nuclei, and in what amounts, are affected by individual nuclear properties. Approach (1) inherently modifies the nucleosynthesis simulation itself, insofar as decay and reaction rates themselves are modified. While approach (2) does not affect nucleosynthesis simulations in the same way, it provides only limited insight into which aspects of a simulated abundance pattern are affected.

In this work, we introduce a new framework for nucleosynthesis modeling, *nucleosynthesis tracing*, that can be applied to supplement these two approaches. Nucleosynthesis tracing enables the robust quantification of which nuclei have participated in an arbitrary collection of nuclear reactions, decays, and/or fission at some point during nucleosynthesis, thereby relating specific nuclear properties to those components of nuclear abundances to which they are connected over the course of nucleosynthesis. In Sec. II, we identify the underlying assumptions of the nucleosynthesis tracing framework and derive the differential equations that define the technique. In Sec. III, we briefly summarize how we have implemented nucleosynthesis tracing as PRISM^tr, a modified version of the nuclear reaction network code Portable Routines for Integrated Nucleosynthesis Modeling (PRISM). Finally, we demonstrate several possible applications of nucleosynthesis tracing to rapid neutron capture (r process) nucleosynthesis in Sec. IV.

II. THEORY

Traditional nuclear reaction networks time evolve the nuclear abundances of a system actively undergoing nucleosynthesis. These calculations require a number of different input parameters, including an initial composition of nuclei and any relevant nuclear properties, such as nuclear reaction and decay rates. Because these rates may depend on the thermodynamics of the system, it is also necessary to specify and evolve the temperature and density during nucleosynthesis. Reaction networks may also incorporate other environmental properties, such as external heating rates and (anti)neutrino fluxes, into their calculations.

The generalized problem of simulating nucleosynthesis may then be phrased as follows. We assume that each nuclide in a system can be uniquely identified by its proton number, Z, and mass number, A. To each combination of these (Z, A), we assign an integer, i, that indexes the species. The number density of species i at any given time is given as n_i, and we define the relative abundance of this species as $Y_i = n_i/\rho N_A$, where ρ is the baryon density, and the mass fractions $X_i = Y_i A_i$ sum to 1, $\sum_i X_i = 1$.

Changes in abundances are enacted by a collection of nuclear transmutation processes, P. For each process p in P, we require the associated quantities listed below.

(1) A rate function Λ_p, which is allowed to depend explicitly on any environmental quantity available to the network, such as temperature, density, or neutrino flux, as appropriate to the process. Insofar as each of these quantities is available to the network as a function of time, the function Λ_p is implicitly a function of time.

(2) A set of nuclear indices, $\mathcal{R}_p$, that correspond to the nuclei consumed by the process.

(3) A set of nuclear indices, $\mathcal{P}_p$, that correspond to the nuclei produced by the process.

(4) A function, $\alpha_p(i)$, that gives the number of species with index $i \in \mathcal{R}_p$ consumed by the process.

(5) A function, $\beta_p(i)$, that gives the average number of species with index $i \in \mathcal{P}_p$ produced by the process.

Once a specific collection of relevant processes, P, is specified, nucleosynthesis is reduced to solving an initial value problem (IVP) for the abundances as a function of time, $Y_i(t)$. The abundances at time t_0 are taken as the initial condition. The set of processes, P, completely defines the system of differential equations for the IVP. For each species in the network, i, the differential equation defining its evolution in time is given as

$$
\frac{dY_i}{dt} = - \sum_{\{p \in P | i \in \mathcal{R}_p\}} \left(\alpha_p(i) \Lambda_p(t) \prod_{j \in \mathcal{R}_p} Y_j(t)^{\alpha_p(j)} \right)
$$
$$
+ \sum_{\{p \in P | i \in \mathcal{P}_p\}} \left(\beta_p(i) \Lambda_p(t) \prod_{j \in \mathcal{R}_p} Y_j(t)^{\alpha_p(j)} \right), \quad (1)
$$

where the first summation is taken over processes in which nuclide i is given in $\mathcal{R}$ and the second over processes in

which nuclide i is given in $\mathcal{P}$. Because our notation differs significantly from more commonly adopted forms, we refer to the Appendix for a description of the relationship between Eq. (1) and that used, e.g., in Ref. [19].

The specific approaches that are taken to solve this IVP vary across reaction networks, and the ideal numerical methods can be application dependent. For simulating r-process nucleosynthesis, a common approach is to solve an implicit Euler equation using the Newton-Raphson method [19–23], although alternative approaches have also demonstrated success [24–29].

A. Nucleosynthesis tracing

In this work, we develop an extension to reaction networks as previously defined. We refer to this extension as a *tracing* reaction network. This extension, which is laid out below, enables the robust quantification of which nuclei in a system have a nucleosynthetic history involving a particular process or processes, among other possible applications.

We begin by constructing a parallel set of abundances to evolve, denoted as $Y_{\text{traced},i}$ and referred to as the *traced abundances*. Physically, the traced abundances identify the subset of the total abundances which have assumed some property, a *trace-in condition*, during nucleosynthesis. Once a nucleus satisfies the trace-in condition, we add it to the traced abundances. We may also wish to remove nuclei from consideration in the traced abundances after they assume some other property, a *trace-out condition*. We otherwise evolve the overall abundances according to Eq. (1) and the traced abundances according to a slightly modified form of the same equation. It is also helpful to define the *untraced* abundances as $Y_{\text{untraced},i} = Y_i - Y_{\text{traced},i}$.

For the present work, we strictly consider trace-in and trace-out conditions to be the participation in a collection of processes, P_{in} and P_{out}, respectively. Effectively, we begin tracing a nucleus once it is produced by a process identified in P_{in}, and we continue to follow it throughout all subsequent nucleosynthesis in which it participates. However, if it is consumed by one of the processes in P_{out}, we remove it from the traced abundances, and we do not consider any further nucleosynthesis in which it participates. We also define an additional set of processes, P_{other}, which we define as the set of those processes in P belonging to neither P_{in} nor P_{out}.

We illustrate schematically how one- and two-body processes in each of P_{in}, P_{out}, and P_{other} affect the evolution of the traced abundances in Fig. 1. Processes in P_{in} and P_{out} are relatively straightforward, as products are always mapped into the traced and untraced populations, respectively. For one-body processes in P_{other}, the mapping is straightforward as well, as products of traced nuclei are mapped into the traced population, and products of untraced nuclei are mapped into the untraced population.

For two-or-more-body processes, the situation is more complicated. If a traced nucleus interacts with a traced nucleus, then the products clearly should be mapped into the traced population. Likewise, if only untraced nuclei undergo the process, then the products unambiguously belong in the
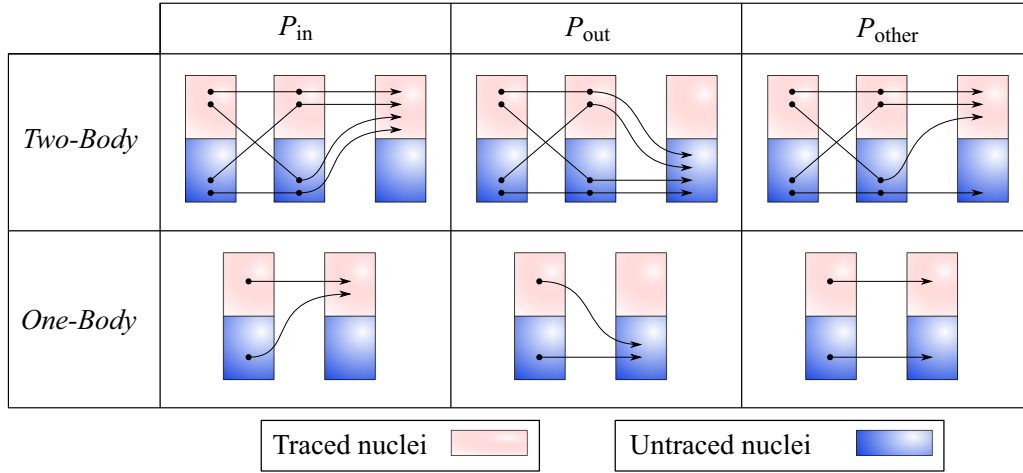
FIG. 1. A schematic diagram of nucleosynthesis tracing. Populations of traced nuclei (top red boxes) and untraced nuclei (bottom blue boxes) interact via one-body and two-body trace-in processes (P_{in}), trace-out processes (P_{out}), and other processes (P_{other}). The filled circles represent nuclei consumed by a process, and the arrowheads represent nuclei produced by a process. For the trace-in processes, products are mapped exclusively to the traced population, while the trace-out processes map products exclusively to the untraced population. All other processes are allowed to map products to either the traced or untraced populations, depending on the populations to which the reactants belong.

untraced population. It is also possible that some number of untraced nuclei interact with some other traced nuclei, and we are forced to choose what fraction of the products belong to the traced and untraced populations. The simplest choice is to assert that if *any* nucleus consumed by the process is traced, then the products are always mapped into the traced population, as can be seen in the top-right panel of Fig. 1. This is the choice we explore in the present work, although other meaningful choices are possible.

The system of differential equations describing the evolution of the traced abundances may now be defined under these assumptions. There are four distinct varieties of terms that present themselves in these differential equations, and we construct each of them in turn.

A traced nucleus, i, is produced by a process, p, in P_{in}. Because we wish to add *all* of the nuclei produced via this process into the traced network, the relevant term should be identical to that of the total abundance Y_i, namely

$$R_1 = \beta_p(i) \Lambda_p(t) \prod_{j \in \mathcal{R}_p} Y_j(t)^{\alpha_p(j)}. \quad (2)$$

A traced nucleus, i, is produced by a process, p, in P_{out}. Because none of the nuclei produced via this process should be mapped into the traced network, this term is simply 0.

A traced nucleus, i, is produced by a process, p, in P_{other}. All nuclei produced by this process should be mapped into the traced network *unless* all of the nuclei involved are untraced. The rate at which *only* untraced nuclei undergo the process is given by

$$R_2' = \beta_p(i) \Lambda_p(t) \prod_{j \in \mathcal{R}_p} Y_{\text{untraced}, j}(t)^{\alpha_p(j)}. \quad (3)$$

The rate at which traced nuclei are produced is the difference between Eq. (2) evaluated for the nucleus produced by process

$p \in P_{\text{other}}$ and Eq. (3),

$$R_2 = \beta_p(i) \Lambda_p(t) \prod_{j \in \mathcal{R}_p} Y_j(t)^{\alpha_p(j)}$$
$$- \beta_p(i) \Lambda_p(t) \prod_{j \in \mathcal{R}_p} Y_{\text{untraced}, j}(t)^{\alpha_p(j)}. \quad (4)$$

Expressed in terms of only traced abundances $Y_{\text{traced}, i}$ and overall abundances Y_i, this reduces to

$$R_2 = \beta_p(i) \Lambda_p(t) \prod_{j \in \mathcal{R}_p} Y_j(t)^{\alpha_p(j)}$$
$$- \beta_p(i) \Lambda_p(t) \prod_{j \in \mathcal{R}_p} [Y_j(t) - Y_{\text{traced}, j}(t)]^{\alpha_p(j)}. \quad (5)$$

A traced nucleus, i, is consumed by a process, p, in P_{in}, P_{out}, or P_{other}. A traced nucleus may interact with any other nucleus, traced or otherwise, to undergo a particular process. As such, the rate at which a traced nucleus is consumed by the process will be in proportion to the overall rate in the ratio $Y_{\text{traced}, i}/Y_i$. The term is given by

$$R_3 = -\frac{Y_{\text{traced}, i}}{Y_i} \left(\alpha_p(i) \Lambda_p(t) \prod_{j \in \mathcal{R}_p} Y_j(t)^{\alpha_p(j)} \right).$$

Because an abundance Y_i may be 0, we rearrange this slightly as

$$R_3 = -\alpha_p(i) \Lambda_p(t) Y_{\text{traced}, i} Y_i^{\alpha_p(i)-1} \prod_{j \neq i \in \mathcal{R}_p} Y_j(t)^{\alpha_p(j)}. \quad (6)$$

The system of equations that govern the traced reaction network is a linear sum of all appropriate terms of the forms

Eqs. (2), (5), and (6), together with the system of equations defined in Eq. (1). It is given by

$$
\frac{dY_i}{dt} = - \sum_{\{p \in P | i \in \mathcal{R}_p\}} \left(\alpha_p(i) \Lambda_p(t) \prod_{j \in \mathcal{R}_p} Y_j(t)^{\alpha_p(j)} \right)
$$
$$
+ \sum_{\{p \in P | i \in \mathcal{P}_p\}} \left(\beta_p(i) \Lambda_p(t) \prod_{j \in \mathcal{R}_p} Y_j(t)^{\alpha_p(j)} \right) \quad (7)
$$

$$
\frac{dY_{\text{traced},i}}{dt} = - \sum_{\{p \in P | i \in \mathcal{R}_p\}} \left[\alpha_p(i) \Lambda_p(t) Y_{\text{traced},i} Y_i^{\alpha_p(i)-1} \right.
$$
$$
\times \left. \prod_{j \neq i \in \mathcal{R}_p} Y_j(t)^{\alpha_p(j)} \right]
$$
$$
+ \sum_{\{p \in P_{\text{in}} | i \in \mathcal{P}_p\}} \left[\beta_p(i) \Lambda_p(t) \prod_{j \in \mathcal{R}_p} Y_j(t)^{\alpha_p(j)} \right]
$$
$$
+ \sum_{\{p \in P_{\text{other}} | i \in \mathcal{P}_p\}} \left[\beta_p(i) \Lambda_p(t) \prod_{j \in \mathcal{R}_p} Y_j(t)^{\alpha_p(j)} \right.
$$
$$
\left. - \beta_p(i) \Lambda_p(t) \prod_{j \in \mathcal{R}_p} [Y_j(t) - Y_{\text{traced},j}(t)]^{\alpha_p(j)} \right]. \quad (8)
$$

This extended system of equations can then be solved using the same numerical techniques as for traditional network equations [Eq. (1)]. Both the total and traced abundances evolve mostly separate from each other, with connections between the two mediated by the P_{in} and P_{out} processes. Note that because the equations for $\frac{dY_i}{dt}$ are the same as in Eq. (1), they are not affected in any way by the extended network, and simulating the total abundances will not be affected by using the extended network equations. However, the total abundances do arise in the equations for the $\frac{dY_{\text{traced},i}}{dt}$, and through this dependence the dynamic interactions of the traced abundances with the total abundances are effectively captured.

III. NUCLEOSYNTHESIS AND PRISM

For the demonstrated applications of the nucleosynthesis tracing framework presented in Sec. IV, we use an updated version of the reaction network code PRISM [17,30,31] denoted as PRISM$^{\text{tr}}$. The extended network equations defining the evolution of the traced abundances, summarized as Eq. (8), are structurally very similar to those of the total abundances, Eq. (7). Numerically, we solve both the total abundances and the traced abundances over a series of discrete time steps by solving an implicit Euler equation using the Newton-Raphson method. In addition to solving for the time derivatives $\frac{dY_i}{dt}$ and $\frac{dY_{\text{traced},i}}{dt}$, this approach requires evaluating the partial derivatives

$$
\frac{\partial}{\partial Y_j} \left(\frac{dY_i}{dt} \right),
$$
$$
\frac{\partial}{\partial Y_j} \left(\frac{dY_{\text{traced},i}}{dt} \right),
$$

$$
\frac{\partial}{\partial Y_{\text{traced},j}} \left(\frac{dY_i}{dt} \right), \text{ and}
$$
$$
\frac{\partial}{\partial Y_{\text{traced},j}} \left(\frac{dY_{\text{traced},i}}{dt} \right).
$$

Insofar as Eqs. (7) and (8) are polynomials of the Y_i and $Y_{\text{traced},i}$, these partial derivatives are straightforward to evaluate, and we do not give their explicit form here.

For the calculations performed in this work, we use PRISM$^{\text{tr}}$ to perform a number of r-process nucleosynthesis tracing simulations. In all cases, we implement a combination of experimental data and theory calculations for charged-particle reaction rates; β^- decay rates; delayed neutron emission probabilities; neutron-capture rates; one-neutron photodissociation rates; neutron-induced, β^--delayed, and spontaneous fission rates; and fission yields. Charged-particle reaction rate data is taken from the JINA REACLIB database [32]. The β^- decay rates, β^--delayed fission rates, and delayed neutron emission probabilities are evaluated using the Los Alamos National Laboratory (LANL) QRPA + HF framework of Refs. [33,34] using AME2016 [35] and FRDM2012 [36] nuclear masses. Neutron-capture rates and neutron-induced fission rates are calculated using the LANL statistical Hauser-Feshbach code COH [37], also assuming AME2016 and FRDM2012 nuclear masses. One-neutron photodissociation rates are evaluated by detailed balance, with the requisite one-neutron separation energies taken from the AME2016 and FRDM2012 nuclear masses. Fission yields are taken from the calculations of Ref. [38]. We implement all decay half-lives and branching ratios of the Nubase 2016 evaluation [39], which are taken to replace the aforementioned theory calculations when possible.

Finally, we note that many of these processes invariably produce one or more free neutrons. We do not, for the present work, intend to trace the nucleosynthesis in which these neutrons participate. In order to prevent such neutrons from populating the traced abundances, we fix $\frac{dY_{\text{traced,neutron}}}{dt} = 0$, instead of evaluating it according to Eq. (8). Future work may investigate, e.g., the relative effect of these neutrons on r-process nucleosynthesis, in which case it would be necessary to evaluate $\frac{dY_{\text{traced,neutron}}}{dt}$ via Eq. (8).

IV. APPLYING THE NUCLEOSYNTHESIS TRACING FRAMEWORK TO THE r PROCESS

The rapid neutron capture process (r process) of nucleosynthesis is the astrophysical mechanism by which the heaviest elements observed to exist in the universe are formed. The r process proceeds by an alternating sequence of neutron capture and β^- decay toward progressively heavier nuclei and is made possible by extremely hot, dense, and neutron-rich environments [1]; identifying the astrophysical events that provide such extreme conditions remains one of the greatest open problems in nuclear astrophysics [40,41]. Major progress toward this goal occurred with the first gravitational wave observation of a neutron star merger, GW170817/GRB170817a/SSS17a [42,43]. Analysis of the electromagnetic counterpart of this event suggests a significant lanthanide component in the ejecta of this event, pointing

to neutron star mergers as one possible site of the r process [44]. However, owing to significant challenges in observational astronomy, astrophysics, and nuclear physics, it is not yet possible to clearly identify neutron star mergers as the dominant source of r-process nuclei in the universe (see, e.g., Refs. [5–7] and references therein).

The r process poses several barriers to analysis that make it a particularly interesting focus for the first application of our tracing framework. Multiple nuclear processes, including neutron capture, neutron photodissociation, and β^- decay, are all in competition as thousands of different nuclear species are populated throughout nucleosynthesis; when some of the heaviest and most neutron-rich nuclei are formed, fission begins to compete as well, populating lighter nuclei according to complex fission fragment distributions (yields) that potentially span hundreds of different nuclei. Because of the large number of nuclear species involved and the numerous transmutation processes connecting them, it can be especially difficult to quantify how individual transmutation processes interact with the many others to determine the progression of nucleosynthesis.

In this section, we demonstrate several ways that our nucleosynthesis tracing framework may be applied to address the challenges associated with understanding the role of nuclear properties in governing r-process nucleosynthesis. Section IV A highlights the role of different fission channels—considered as a whole, as well as for individual nuclei—in a variety of neutron star merger r-process environments. In Sec. IV B, we choose a set of neutron star merger wind conditions where fission plays a minimal role and perform tracing calculations for the β^- decay of elements $40 \leqslant Z \leqslant 80$.

A. Distribution of fission products in final r-process abundances

In extremely neutron-rich environments, sufficiently heavy nuclei may be formed during the r process such that these nuclei begin to fission, with varying degrees of significance for the nuclear abundances produced from nucleosynthesis. In the most extreme cases, fission recycling may occur, in which the bulk of nuclei undergo fission; these nuclei are returned to lighter nuclei and undergo additional neutron captures and β^- decays characteristic of the r process. In such conditions, the specific nuclear abundances are expected to depend on the fission properties of many exotic neutron-rich nuclei [17,18,45–49]. However, these fission properties effectively rely entirely on theory-based predictions, and a great deal of progress has been made to evaluate them, including from systematic, macroscopic-microscopic, and purely microscopic theoretical approaches (see, e.g., Ref. [50] and references therein for a recent review; also Refs. [17,18,38,51–54]). In order to help inform existing and future efforts in the study of nuclear fission, we use our tracing framework to examine the various ways that different fission processes, namely spontaneous fission (sf), β^--delayed fission (βdf), and neutron-induced fission (n, f), can influence r-process nucleosynthesis in the ejecta of a neutron star merger.

For this analysis, we begin by selecting a set of three trajectories that broadly represent the varying extents to which
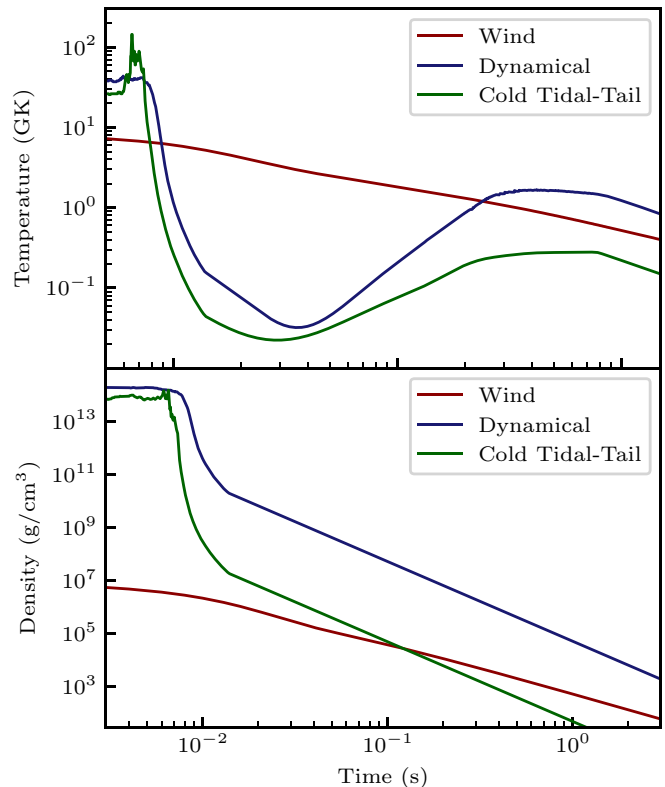

FIG. 2. Comparison of temperature (upper panel) and density (lower panel) profiles used in this work to explore the contributions of fission products in different types of neutron star merger ejecta: wind ejecta (red lines), for which fission plays a subdominant role during nucleosynthesis; dynamical ejecta (blue lines), in which most, but not all, nuclei participate in fission; and cold dynamical ejecta (green lines), in which nearly all nuclei undergo fission one or more times.

fission contributes to nucleosynthesis, enumerated below as follows:

(1) Parameterized accretion-disk wind ejecta conditions, with timescale $\tau = 20$ ms, initial specific entropy $s = 40 \, k_B$/baryon, and electron fraction $Y_e = 0.20$, as used in Ref. [31].

(2) Dynamical ejecta of a binary neutron star merger conditions taken from the simulations of Refs. [46,55,56], with initial specific entropy $s = 0.62 \, k_B$/baryon and electron fraction $Y_e = 0.049$.

(3) Cold tidal-tail ejecta of a binary neutron star merger conditions, similarly taken from the simulations of Refs. [46,55,56], with initial specific entropy $s = 4.3 \, k_B$/baryon and electron fraction $Y_e = 0.019$.

In Fig. 2, we compare the temperature and density profiles for each of these trajectories. The wind conditions have much higher entropy and electron fraction than either of the two dynamical ejecta trajectories, leading to conditions that support much less fission overall. The two dynamical ejecta conditions are more similar to each other, with extremely low entropies and electron fractions that are considerably more suited for the production of fissioning nuclei, the effects of which can

be clearly seen in the dramatic increase in temperature that occurs beginning around 0.01 s, reflecting the considerable release of nuclear energy from fission that heats the system. While qualitatively very similar, the overall lower density, temperature, and initial electron fraction of the cold tidal-tail ejecta is expected to lead to substantially higher levels of fission, which we explore in more detail later on in this section.

In order to assist in the analysis and interpretation of these tracing calculations, it is also helpful to consider the abundance-weighted average timescales [16] of the dominant classes of transmutation processes taking place during nucleosynthesis, which we identify here as neutron capture (n, γ) and the inverse process (γ, n); nuclear β^- decay; and the fission processes βdf and (n, f). For each of these, we define the abundance-weighted timescale τ by

$$\tau_{(n,\gamma)} = \sum_i Y_i \bigg/ \sum_i Y_n Y_i \Lambda_{(n,\gamma),i},$$

$$\tau_{(\gamma,n)} = \sum_i Y_i \bigg/ \sum_i Y_i \Lambda_{(\gamma,n),i},$$

$$\tau_{\beta^-} = \sum_i Y_i \bigg/ \sum_i Y_i \Lambda_{\beta^-,i}, \tag{9}$$

$$\tau_{\beta df} = \sum_i Y_i \bigg/ \sum_i Y_i \Lambda_{\beta df,i}, \text{ and}$$

$$\tau_{(n,f)} = \sum_i Y_i \bigg/ \sum_i Y_n Y_i \Lambda_{(n,f),i},$$

where the summations over nuclear species i are restricted to heavy nuclei, Y_n is the free neutron abundance, and the Λ_i are the rate functions of Eq. (1). These abundance-weighted timescales represent the average timescale for a nucleus to proceed through each of the five nuclear transmuation processes, where lower values of τ correspond to comparatively faster rates and vice versa.

We plot the timescales for each of the three astrophysical conditions as a function of time in Fig. 3. Several basic aspects of the r process clearly emerge in each case, in particular (1) an early phase where (n, γ) and (γ, n) reactions clearly dominate as the fastest processes in the network and proceed in equilibrium, as indicated by the equality of $\tau_{(n,\gamma)}$ and $\tau_{(\gamma,n)}$; (2) the point of freeze-out, at which β^- decay surpasses (n, γ) as the fastest process, i.e., when τ_{β^-} intersects with $\tau_{(n,\gamma)}$; and (3) a decay toward stability phase that occurs following freeze-out, where the unstable nuclei formed during the r process undergo a series of decays to stable nuclei. As can also be inferred from the timescales, nuclear fission may take place at various points and to varying degrees during the r process.

In the case of of the wind ejecta, fission timescales are fastest ($\tau \approx 100$ s) sometime around freeze-out and persist throughout the decay-to-stability phase, such that all fission products predominantly undergo β^- decay toward stability, although they may also undergo some number of latent (n, γ) or (γ, n) reactions as well.

In the dynamical and cold tidal-tail ejecta conditions, fission arises much sooner and occurs over much faster
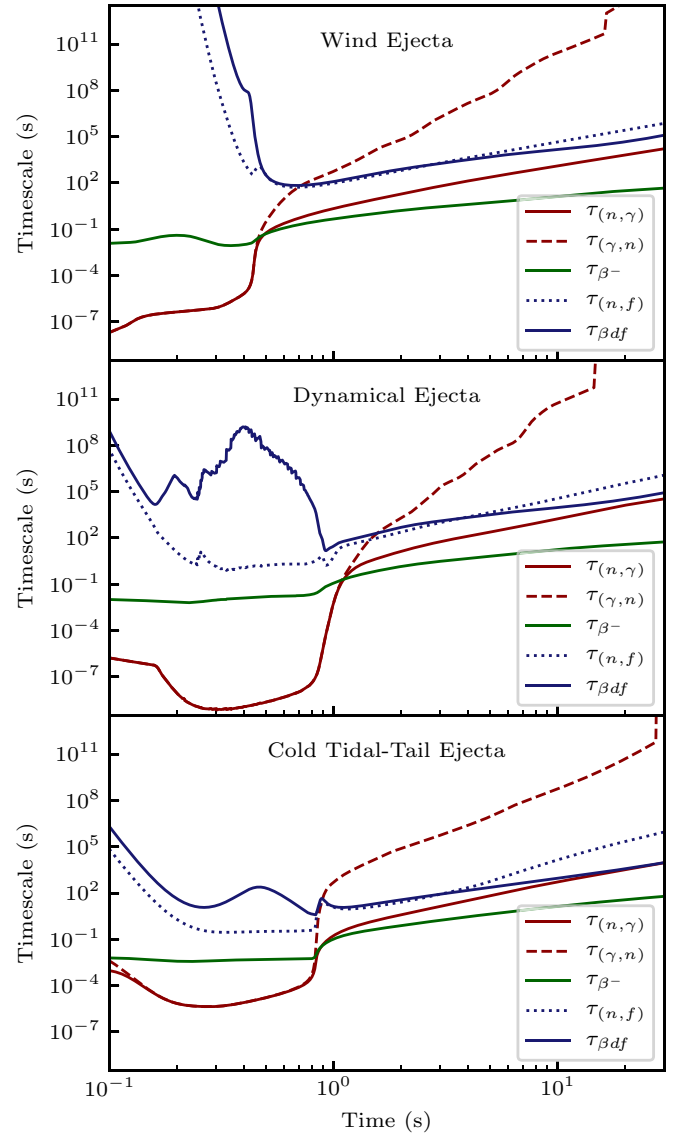

FIG. 3. For each of the parameterized wind ejecta (top), dynamical ejecta (middle), and cold tidal-tail ejecta (bottom), the average timescales for (n, γ) (solid red) and (γ, n) (dashed red); β^- decay (solid green); and βdf and (n, f) fission channels (dotted and solid blue lines, respectively).

timescales ($\tau \approx 1$ s) in comparison with the wind ejecta. In these examples, fission products may also be significantly produced before freeze-out. These fission products will be re-equilibrated into the r-process path via the $(n, \gamma) \rightleftharpoons (\gamma, n)$ equilibrium, where they will continue to be processed into heavier nuclei until freeze-out occurs, a process described as *fission recycling*.

While timescales provide an excellent basis for providing a broad description of fission's role in nucleosynthesis, we demonstrate how our nucleosynthesis tracing framework can be applied to quantitatively describe how fission products contribute to specific features of r-process abundances. For our first analysis, we perform three separate nucleosynthesis tracing calculations, in which the products of all nuclei
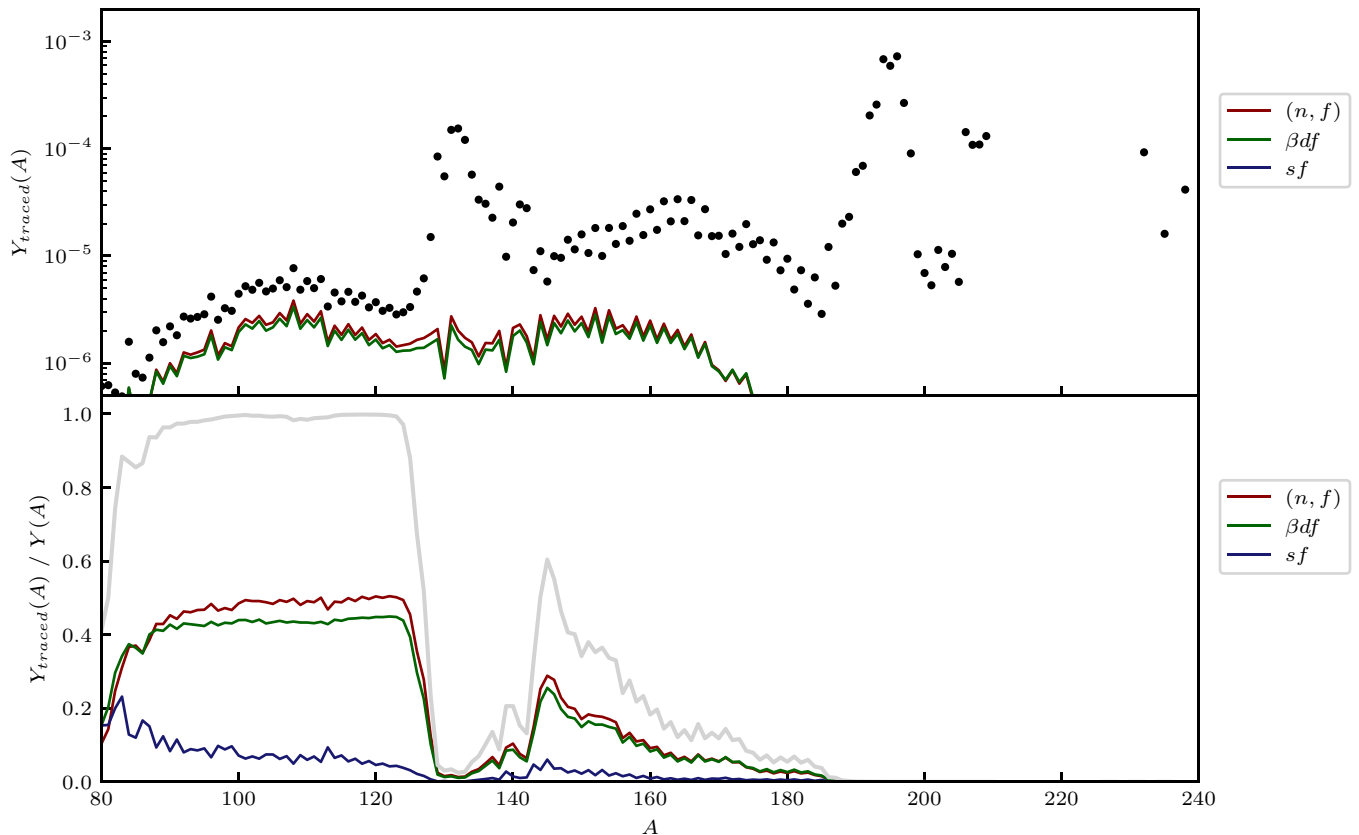
FIG. 4. Relative contributions to final isotopic abundances by terminating fission channel (spontaneous fission, sf; neutron-induced fission, (n, f); and β^--delayed fission, βdf) for the neutron star merger wind conditions described in the text. The top panel compares the traced abundances (solid lines) to the total abundances (dots). The bottom panel shows the ratio of each traced abundance to the total abundance; the gray line indicates their sum. For $A < 125$, all abundances are populated almost exclusively by fission processes, while the relative contributions to $A > 125$ are comparatively weaker, peaking at $\approx 50\%$.

fissioning via a particular channel, (n, f), βdf, or sf, are followed throughout the remaining nucleosynthesis. Because some heavy nuclei may have been processed through more than one fission event, we restrict the current analysis to the final, or terminating, fission event by setting a trace-out condition for the two remaining fission channels. In this way, we perform three tracing calculations for each of the three astrophysical conditions.

We begin by considering the wind ejecta conditions, where fission is expected to play a subdominant role, as previously discussed. The results of each of our three tracing calculations, i.e., for each of the (n, f), βdf, and sf fission channels, are shown in Fig. 4. The contributions are dominated by the (n, f) and βdf channels, with the final distribution of fission products lying in the $80 < A < 180$ region. Among the fission contributions to the overall pattern, roughly equal contributions arise from the (n, f) and βdf channels. In particular, we note that for these conditions, very few nuclei remain to the left of the second r-process peak ($A \approx 130$) prior to the onset of fission, with contributions to this region being dominated by material that is directly deposited there as fission products. Because this fission occurs relatively late during nucleosynthesis, around the point of freeze-out and throughout the subsequent decay-to-stability phase of nucleosynthesis, as can be seen in Fig. 3 and the supporting discussion, the material

does not significantly move forward into the second or third ($A \approx 195$) peaks via subsequent neutron capture.

We repeat this analysis for our selected dynamical ejecta conditions. Fission is more significant in this case, with around 60–80% of heavy nuclei across the entire pattern having participated in fission. Furthermore, significant amounts of (n, f) products undergo follow-up neutron-capture nucleosynthesis, forming up to 60% of abundances well beyond the extent of the fission yields, including the third r-process peak and long-lived actinide isotopes. These contributions arise from earlier stages of nucleosynthesis, when (n, γ) and (γ, n) reactions dominate the other available transmutation processes, between 0.2 and 1 s as demonstrated by the timescales in Fig. 3. As such, these early-time fission products will re-integrate into the r-process path determined by the equilibrium between (n, γ) and (γ, n) and be subsequently processed into heavier nuclei.

Nuclei to the left of the second peak are populated via a mechanism similar to that of the wind conditions from Fig. 4. Toward the end of nucleosynthesis, after freeze-out has occurred around 1 s, the free neutron abundance is sufficiently low such that β^- decay proceeds more quickly, on average, than (n, γ) reactions. Because of this, contributions in the $80 < A < 125$ region arise from the late-time (n, f) and βdf
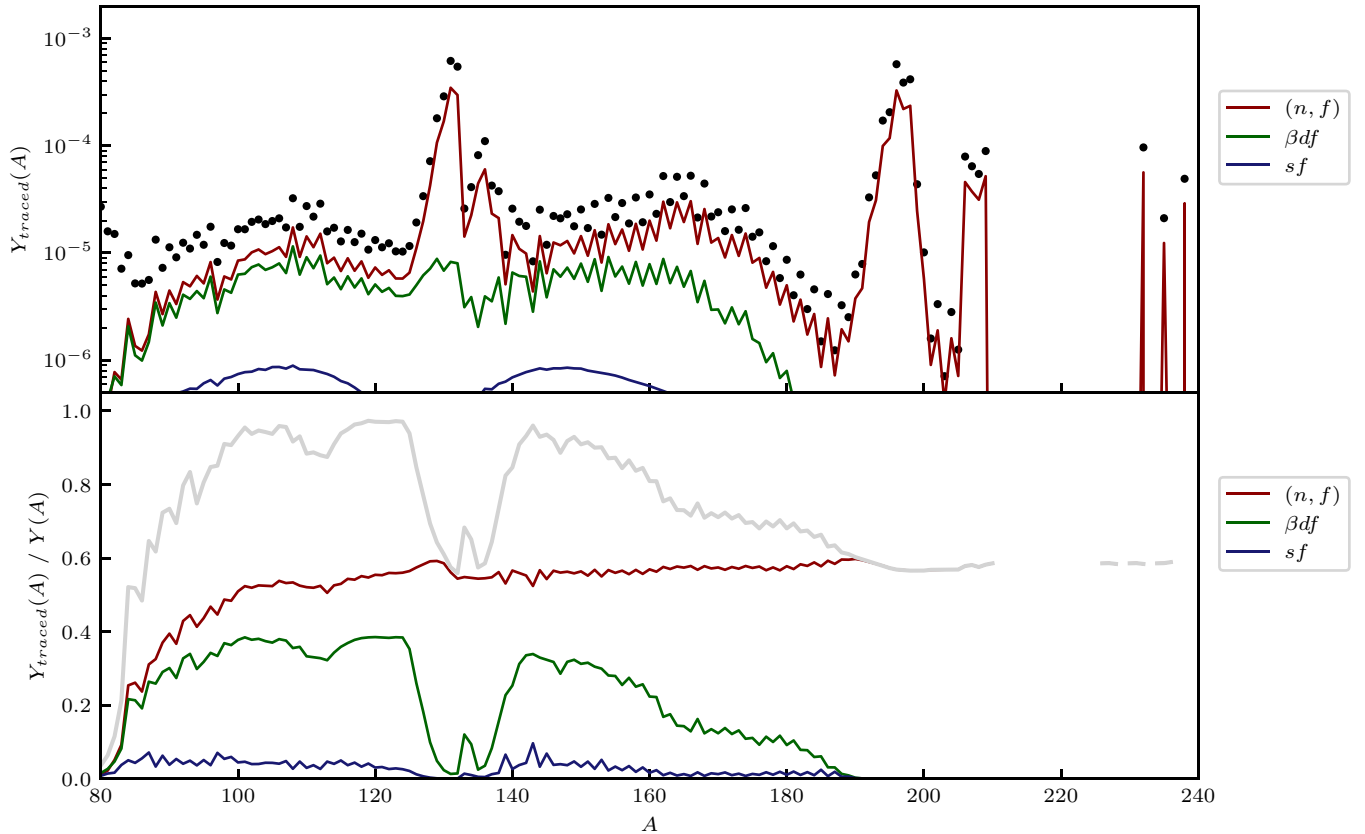
FIG. 5. Relative contributions to final isotopic abundances by terminating fission channel (spontaneous fission, sf; neutron-induced fission, (n, f); and β^--delayed fission, βdf) for dynamical ejecta conditions from a neutron-star merger simulation [46,55,56], as in Fig. 4. For these conditions, nucleosynthesis proceeds via incomplete fission recycling, with neutron-induced fission accounting for $\approx 60\%$ of abundances across the entire range of the pattern, and β^--delayed fission accounting for an additional 10% to 30% for $A < \sim 180$. The remaining abundances, about 10% to 40% depending on A, have no history of fission.

fission products whose isotopic distributions do not appreciably change due to (n, γ) reactions.

Finally, we consider our selected cold tidal-tail ejecta conditions. Here, all heavy nuclei have been processed one or more times through fission, possibly via multiple fission channels. For our analysis, we consider only contributions that arise from the terminating, or last, fission event. In order to achieve this, we trace in all fission events for the particular channel under consideration and trace out all other fission events. If a particular abundance in the final pattern has a history involving two different fission channels, only the contribution from the last fission event is considered. As can be seen in Fig. 6, the effect of this is that the sum of fission traces across the (n, f), βdf, and sf channels add neatly to unity, even though the average nucleus has more than one fission event in its history.

In contrast with the calculations shown in Fig. 5, βdf also becomes active during earlier phases of nucleosynthesis before freeze-out occurs (0.2 to 0.8 s, as indicated by the timescales in Fig. 3), and βdf competes with (n, f) for fissionable nuclei populated during this phase of nucleosynthesis. As evidence of this, note that the βdf products are able to undergo further neutron capture reactions, eventually populating $\approx 10\%$ of the third peak and long-lived actinide abundances, in addition to some movement of the

products from the $A < 125$ region into the second peak. As with the previous conditions, nuclei to the left of the second peak are dominated by late-time fission products produced after freeze-out around 0.8 s, with roughly equal contributions from the (n, f) and βdf channels.

As a final point of discussion for our first set of tracing calculations, we point out that these calculations provide an alternative approach to characterizing the extent of fission recycling (also sometimes referred to as fission cycling) in r-process environments. Past approaches have focused on counting the number of fission cycles by comparing the sum total of nuclear abundances before and after nucleosynthesis, taking into account the fact that when nuclei fission into two fragments, their total abundance effectively double (e.g., as in Refs. [57,58]).

Our nucleosynthesis tracing calculations approach the description of fission recycling from a slightly different perspective by quantifying the specific fraction of individual nuclear abundances that have proceeded through fission at *any* point in their history. In this way, these calculations determine whether the final set of nuclear abundances, in their entirety, have been completely processed through fission one or more times (as in the cold tidal-tail conditions, Fig. 6) or only partially (as in the dynamical conditions, Fig. 5). In the former case, we denote the r process as having undergone *complete*
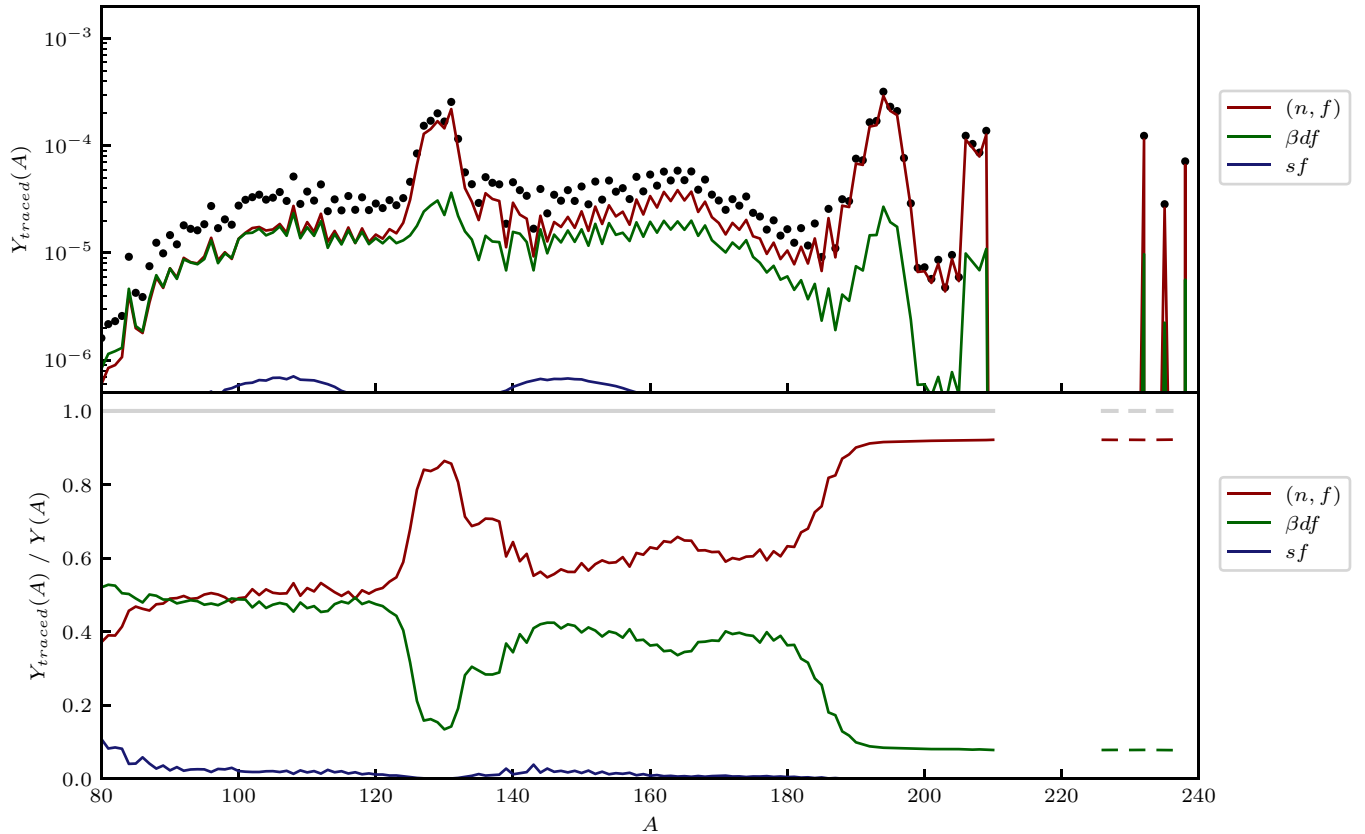
FIG. 6. Relative contributions to final isotopic abundances by terminating fission channel (spontaneous fission, sf; neutron-induced fission, (n, f); and β^--delayed fission, βdf) for the cold tidal-tail ejecta conditions from a neutron star merger simulation [46,55,56], as in Figs. 4 and 5. Under these conditions, nucleosynthesis proceeds via complete fission recycling, with 100% of the pattern having a traced history involving (n, f), βdf, or sf.

fission recycling, and in the latter case, as having undergone *incomplete* fission recycling. In contrast with existing definitions based on the enumeration of fission cycles *on average*, our definition provides a dichotomous classification of fission's role in the r process. In this sense, the two approaches are complementary to each other.

While valuable insight can be derived from tracing entire fission channels across all nuclei, it is also possible to apply our tracing technique with much finer resolution by tracing the fission of individual nuclei. While integrated fission flows have helped inform which nuclei most actively undergo fission during the r process (see, e.g., Refs. [17,18]), such approaches provide limited information relating to the distribution of the fission products throughout the abundance pattern at the conclusion of nucleosynthesis. These effects become particularly important in conditions for which nucleosynthesis proceeds via complete or incomplete fission recycling, where there is a combination of early-time fission (whose products are significantly reprocessed via neutron capture), late-time fission (whose products are mostly restricted to β^- decays toward stable nuclei), and intermediate cases.

We perform tracing calculations for the (n, f) and βdf of each nuclide found to fission in the cold tidal-tail ejecta considered in Fig. 6 and appurtenant discussion. While $\approx$300 nuclides fission via either channel during nucleosynthesis,

we find that the overall contribution of their products to the final calculated abundances is quite small for the majority of these, on the order of 1% or less. By restricting to fission processes with traced abundances constituting a minimum of 10% of the final pattern for at least one value of A, we find nine fission processes to surpass this threshold, distributed across very neutron-rich neptunium ($Z = 93$) and plutonium ($Z = 94$) isotopes populated during the period leading up to freeze-out (between 0.2 and 0.8 s; see Fig. 3). Collectively, the fission of these nuclei drive the effects of early-time fission events presented in the discussion of Fig. 6.

In Fig. 7, we plot the traced abundances for each of these nine fission processes. In each case, the traced abundances follow the same shape as the total pattern, suggesting that the fission products from these nuclei do not imprint on the final abundance pattern, instead quickly re-equilibrating along the r-process path via the $(n, \gamma) \rightleftharpoons (\gamma, n)$ equilibrium—an interpretation consistent with that of Fig. 6. To reinforce this point, we compare the actual fission yield with the traced abundances for the most-significantly fissioning (n, f) nuclide, neptunium-290, in Fig. 8. While the fission yield is smoothly distributed along $90 < A < 190$, the products are eventually redistributed throughout the second and third r-process peaks and long-lived actinide isotopes, in proportion to the total abundance pattern. We re-emphasize that even though the traced abundances of these $\approx$9 fission processes
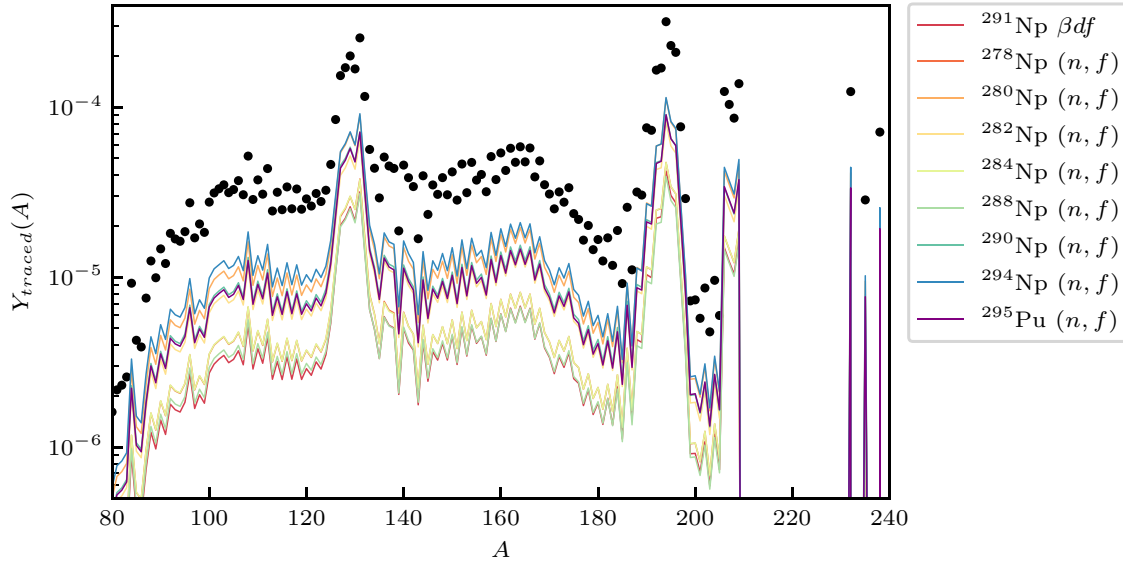
FIG. 7. Relative contributions to final isotopic abundances, $[Y(A)$, solid dots] for the β^--delayed (βdf) and neutron-induced $[(n, f)]$ fission products of individual neptunium and plutonium isotopes (solid lines) in the cold tidal-tail ejecta conditions of Refs. [46,55,56], as in Fig. 6. The plotted isotopes are those whose fission yields contribute at least 10% to the total abundance pattern for at least one mass number A.

are large in magnitude with respect to the total abundances, this does not necessarily indicate that the specific properties of these fission processes are directly responsible for shaping the final abundance pattern, as these fission products are quickly reintegrated into $(n, \gamma) \rightleftharpoons (\gamma, n)$ equilibrium, which is determined by nuclear structure considerations of lighter nuclei.

Some fraction of material processed through these ≈ 9 early-time fission processes will eventually undergo a final late-time fission event sometime after freeze-out occurs. Consequently, nuclei will be distributed according to the yields of these final fission events without significant reprocessing by neutron capture. Because these calculations continue to trace fission products through all subsequent fission events,

we see the formation of the $80 < A < 125$ abundances in Fig. 7. Our tracing calculations suggest that, for an r process proceeding via complete fission recycling, abundance features which eventually form via late-time fission were first processed through the fission of just a handful of nuclear species, in this particular case the ≈ 9 fission processes we have identified here.

If we consider nuclei that fission below the 10% threshold used in the preceding discussion, we find a large number of late-time fission processes whose yields leave a static imprint on the total abundance pattern. In Fig. 9, we compare the fission yield to the traced abundances for one such example, the late-time βdf of berkelium-270 ($Z = 97$). The traced abundances, in this case, clearly follow the fission yield, with any discrepancies arising from β^--delayed neutron emission
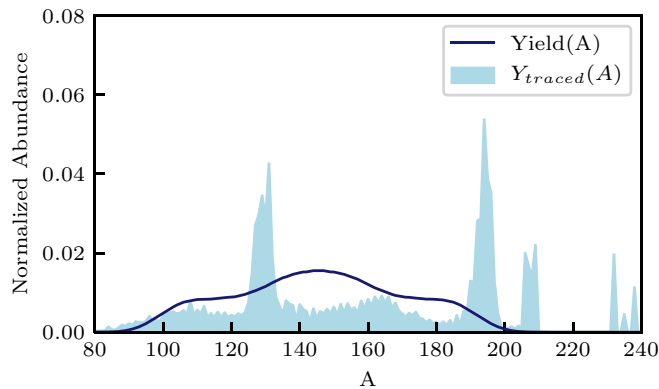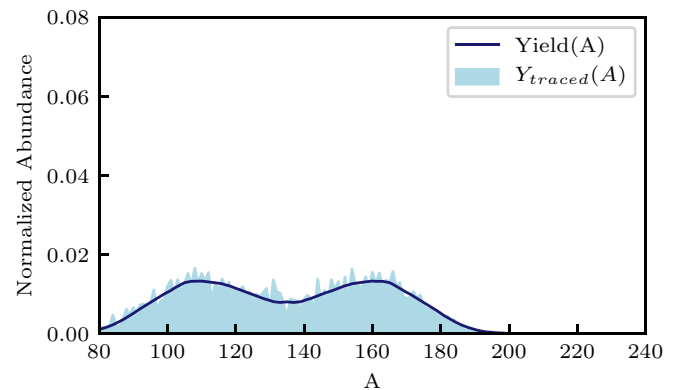

FIG. 8. Comparison of fission yield (solid line) to final traced abundances (shaded region) for the neutron-induced fission of neptunium-290 in the cold tidal-tail ejecta conditions of Refs. [46,55,56], as in Fig. 6. Both are normalized according to Eq. (12). Nuclei produced by this fission process participate in significant further neutron-capture nucleosynthesis, with the actual fission yield leaving a minimal imprint on the final abundance pattern.

FIG. 9. Comparison of fission yield (solid line) to final traced abundances (shaded region) for the β^--delayed fission of berkelium-270, as in Fig. 8. Nuclei produced by this fission process primarily undergo a series of β^- decays, with minimal effect on the distribution in mass number, A, compared to that of the original yield.
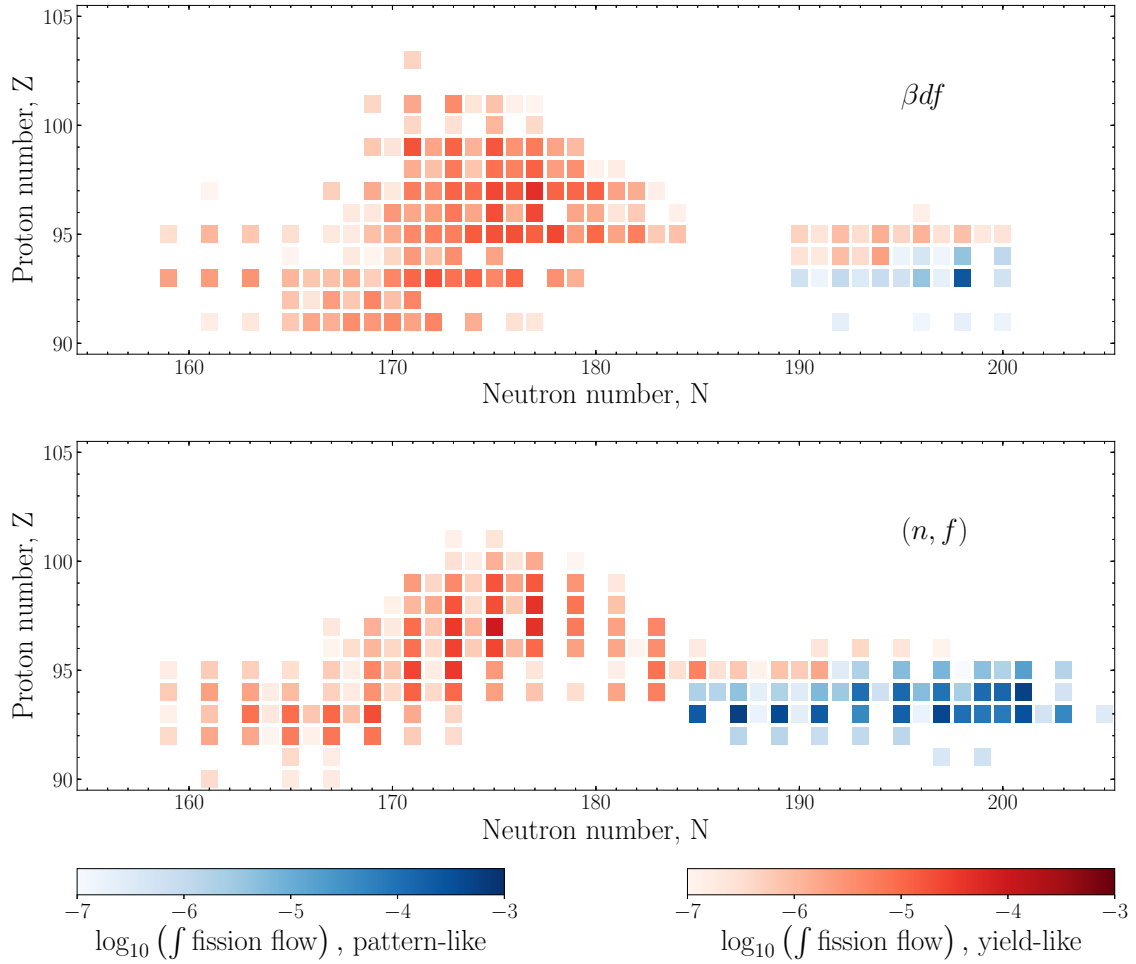
FIG. 10. Integrated β-delayed (βdf, top panel) and neutron-induced ((n, f), bottom panel) fission flows for individual nuclides during the cold tidal-tail ejecta conditions of Refs. [46,55,56], as in Fig. 6. Red color indicates that the traced isotopic abundances are mostly similar to the fission yield [$Y_{\text{traced}}(A) \sim \text{Yield}(A)$, as in Fig. 9], and blue color indicates that the traced isotopic abundances are similar to the overall pattern [$Y_{\text{traced}}(A) \sim Y(A)$, as in Fig. 8].

that happens as the products decay toward stable nuclei, effectively shifting some of the products toward lower values of A.

Figure 10 places the (n, f) and βdf of each nuclide into the dichotomy of *pattern-like* (as in Fig. 8) and *yield-like* (as in Fig. 9) traced abundances. We begin by calculating integrated fission flows, defined for each nuclide i as $\int \Lambda_{(n,f),i} Y_n Y_i \, dt$ and $\int \Lambda_{\beta df,i} Y_i \, dt$ for (n, f) and βdf, respectively; here, Λ is as defined in Sec. II. For every fission process with an integrated fission flow in excess of 10^{-7}, we evaluate the functions

$$L_{\text{pattern}} = \frac{1}{2} \sum_{A>80} |Y(A) - Y_{\text{traced}}(A)| \qquad (10)$$

$$L_{\text{yield}} = \frac{1}{2} \sum_{A>80} |\text{Yield}(A) - Y_{\text{traced}}(A)| \qquad (11)$$

where $Y(A)$, $Y_{\text{traced}}(A)$, and $\text{Yield}(A)$ are the total abundances, traced abundances, and fission yields, respectively, and each

is normalized such that

$$\sum_{A>80} Y(A) = 1,$$

$$\sum_{A>80} \text{Yield}(A) = 1, \text{ and}$$

$$\sum_{A>80} Y_{\text{traced}}(A) = 1. \qquad (12)$$

In this way, L_{yield} is nearly zero if the traced abundances follow the same distribution as the corresponding fission yield. Likewise, L_{pattern} is nearly zero if the distribution of the traced abundances follows that of the total abundances. By comparing L_{yield} to L_{pattern}, we may systematically identify whether the (n, f) and βdf of each nuclide is pattern-like or yield-like. In Fig. 10, the (n, f) and βdf traced abundances for each nuclide are colored red if they are yield-like and blue if pattern-like, and the shading of each indicates integrated fission flow.
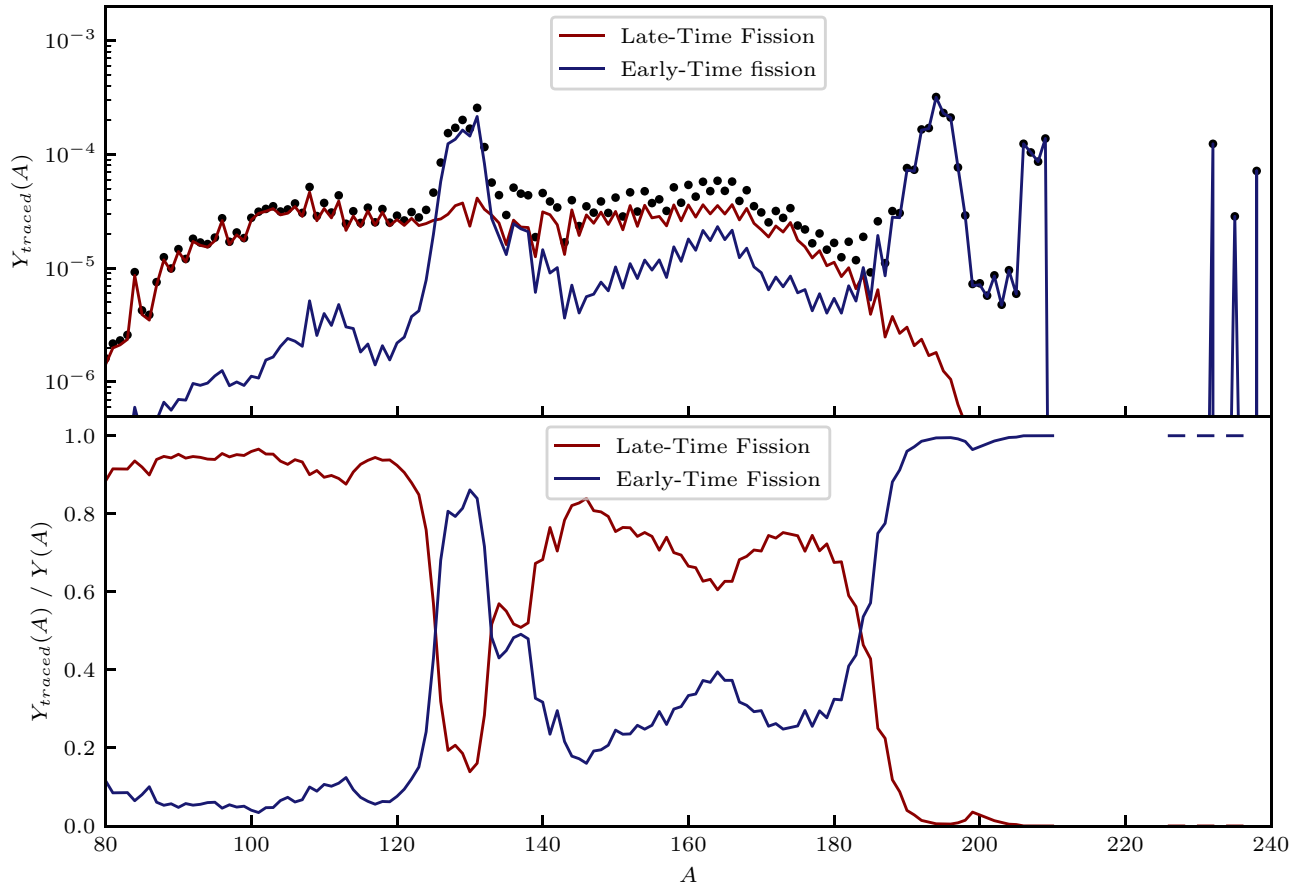
FIG. 11. Separation of nuclear abundances (black dots) for the cold tidal-tail ejecta of Refs. [46,55,56] between those produced directly as fission products after freeze-out (red lines) and those whose last fission event occurred before freeze-out (blue lines), when (n, γ) reactions were sufficiently active to shift their mass distribution toward substantially heavier nuclei.

Along the r-process path ($Z = 93$, 94 and $N \geqslant 185$), all of the traced abundances are pattern-like, confirming that these fission products, by virtue of being populated *before* freeze-out, quickly re-equilibrate along the existing r-process path via $(n, \gamma) \leftrightharpoons (\gamma, n)$ equilibrium. For the remaining less neutron-rich nuclides, which are only populated after freeze-out and therefore dominated by β^- decay in subsequent nucleosynthesis, the traced abundances are consistently yield-like, and their contribution to the overall isotopic abundances are mostly in proportion to their respective fission yields.

The yield-like nuclides for βdf and (n, f) are distributed over a relatively large number of nuclides. Collectively, their fission products play a significant role in shaping certain features of the final abundance pattern. In order to highlight their cumulative effect, we sum over their individual traced abundances to compare their collective contribution to final abundances in Fig. 11. To the left of the second peak ($A < 120$) and between the second and third peaks ($140 < A < 180$), between 60% and 95% of the total nuclear abundances were populated by one of the late-time fission processes indicated by the blue squares of Fig. 10, making their fission products (considered as a whole) the dominant contributors to these regions of the abundance pattern. On the other hand, the effects of individual fission yields are averaged out across these many different nuclides. Indeed, in no case do any of

the traced abundances of these late-time fission processes constitute more than $\approx 7\%$ of the total abundances for any value of A.

While the early-time fission of the most neutron-rich nuclei tends to be more significantly focused on only a few nuclei, these contributions tend to be pattern-like and, therefore, largely insensitive to their associated yields, as their fission products are redistributed via the specific details of the $(n, \gamma) \leftrightharpoons (\gamma, n)$ equilibrium at the time of their production, as well as nuclear-structure-specific features (e.g., $N = 84$, 126 shell closures) that induce the formation of the second, rare-earth, and third r-process peaks that are clearly represented in the early-time fission contributions shown in Fig. 10.

B. Tracing β^- decays in an r process

Because the r process involves the most neutron-rich nuclei, many of these nuclei are difficult to study experimentally, and nucleosynthesis simulations rely heavily on predictions from theoretical nuclear models. Beyond the limits of experimental data, theoretical predictions for these nuclei diverge [59–61], introducing a significant source of uncertainty in r-process nucleosynthesis simulations [10–12,15]. Experimental campaigns at current and upcoming facilities such as CAlifornium Rare Isotope Breeder Upgrade (CARIBU)

[62–67] and the $N = 126$ Factory [68] at Argonne Tandem Linear Accelerator System (ATLAS), Ion Guide Isotope Separator On-Line (IGISOL) at Jyväskylä [69,70], Isotope mass Separator On-Line facility (ISOLDE) at CERN [71], TRIUMFs Ion Trap for Atomic and Nuclear science (TITAN) at TRIUMF [72], RIKEN [73–75], Gesellschaft für Schwerionenforschung (GSI)/Facility for Antiproton and Ion Research (FAIR) [76–78], and Facility for Rare Isotope Beams (FRIB) [79] are approaching nuclei of interest to the r process.

In this context, it will be especially important to identify which nuclei are of critical importance to understanding and constraining r-process nucleosynthesis simulations. Past work has provided sensitivity studies of various nuclear properties entering into r-process calculations, with the goal of identifying how simulated nuclear abundances respond to prescribed changes to these nuclear properties within reasonable estimates for their uncertainties [80]. However, these sensitivity studies face a number of considerable challenges associated, for example, with how to reliably estimate the uncertainties that exist in the nuclear data underlying nucleosynthesis simulations [59–61] and with how to vary the uncertain nuclear data in meaningful ways that capture, e.g., the ways that *individual* points of nuclear data might affect *other* data through correlated effects.

Nucleosynthesis tracing offers a way to examine the relationship between nuclear data and nucleosynthesis *in situ*, insofar as it identifies which nuclear abundances, and in what amounts, are tied directly to specific pieces of nuclear data *without* requiring that the nuclear data itself be adjusted in any number of possible ways. While this does not directly estimate how a given abundance pattern will *change* if some of the nuclear data are also changed, it does provide insight into which abundances, and in roughly what amounts, specific pieces of nuclear data are liable to affect. We note that it may be the case that nucleosynthesis is relatively insensitive to some nuclear transmutation process despite a large abundance being traced through it and vice versa. Therefore, proper sensitivity studies remain an important tool for identifying important nuclear properties needed to constrain nucleosynthesis, and the two approaches are best used together, where the results of each complement the other, to provide a focus for future experimental efforts.

In this first study, we focus specifically on only one category of nuclear data on which r-process nucleosynthesis simulations critically depend, namely β^- decay properties for neutron-rich nuclei. Nuclear β^- decay is the transmutation process responsible for moving neutron-rich nuclei toward heavier elements during the r process. In addition to controlling the number retained at waiting points associated with closed neutron shells, β^- decay can also compete with (n, γ) and (γ, n) reactions to adjust the nuclear abundances produced during the r process for as long as these reaction channels remain active (see, e.g., Refs. [16,81–85]). We focus on identifying which of these β^- decays an r process most significantly passes through.

To simplify the interpretation of our results, we select a single parameterized neutron star merger wind in which fission does not participate as an active process during nucleosyn-
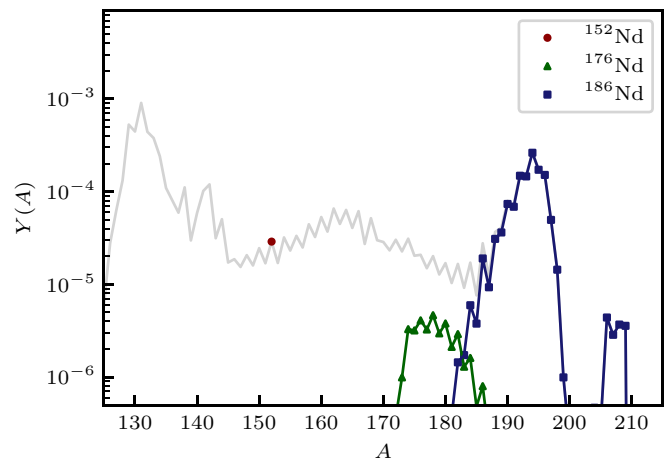

FIG. 12. Traced isotopic abundances for the β^- decay of a selection of neodymium isotopes (neodymium-152, red circle; neodymium-176, green triangles; and neodymium-186, blue squares). The total abundances are given by the gray line for comparison. Neodymium-152 is populated as nuclei are decaying to stable nuclei, and the entirety of abundances for $A = 152$ have undergone this β^- decay. Neodymium-186 lies on the r-process path, and all nuclei with $A \geqslant 186$ have undergone this β^- decay. Neodymium-176 represents an intermediate case, where some fraction, $\approx 10\%$, of nuclei with $A \approx 176$ having been produced by this β^- decay.

thesis, with parameters $s/k_B = 50$, $\tau = 50$ ms, and $Y_e = 0.25$. For each nuclide with $40 \leqslant Z \leqslant 80$ populated at any point during nucleosynthesis, we perform a tracing calculation for its β^- decay. The resulting calculation indicates the relative fraction of each abundance with a history involving the β^- decay under consideration.

The traced β^- decays can be roughly sorted into three distinct, yet physically intuitive, categories. For nuclides nearest stability, their β^- decays occur well after the free neutron abundance has been exhausted, and so these preserve the mass number A with respect to the final pattern. Along the r-process path, the most neutron-rich isotopes populated during an r process, the bulk of of all heavier nuclei will proceed through these nuclei via β^- decay. As a result, the traced abundances will reproduce nearly the entire pattern for all larger values of A. Finally, one can imagine an intermediate case, where nuclei begin to fall back toward stability as a result of decreasing free neutron abundances but may still participate in some degree of neutron capture. To illustrate each of these three regimes, we choose as examples three isotopes of neodymium and show traced abundances for their β^- decays in Fig. 12. In the case of neodymium-152, all of the abundances in the final overall pattern have participated in this β^- decay while decaying back to stability after the completion of the r process. For neodymium-186, which lies along the r-process path, the majority of populated nuclear species with $A \geqslant 186$ have participated in this particular β^- decay. Finally, we highlight the intermediate case with neodymium-176, lying between stability and the r-process path, where some fraction of abundances for multiple nearby A have a history involving this β^- decay.

In Fig. 13, we quantify average trends that arise in these tracing network calculations. For each traced pattern, we de-
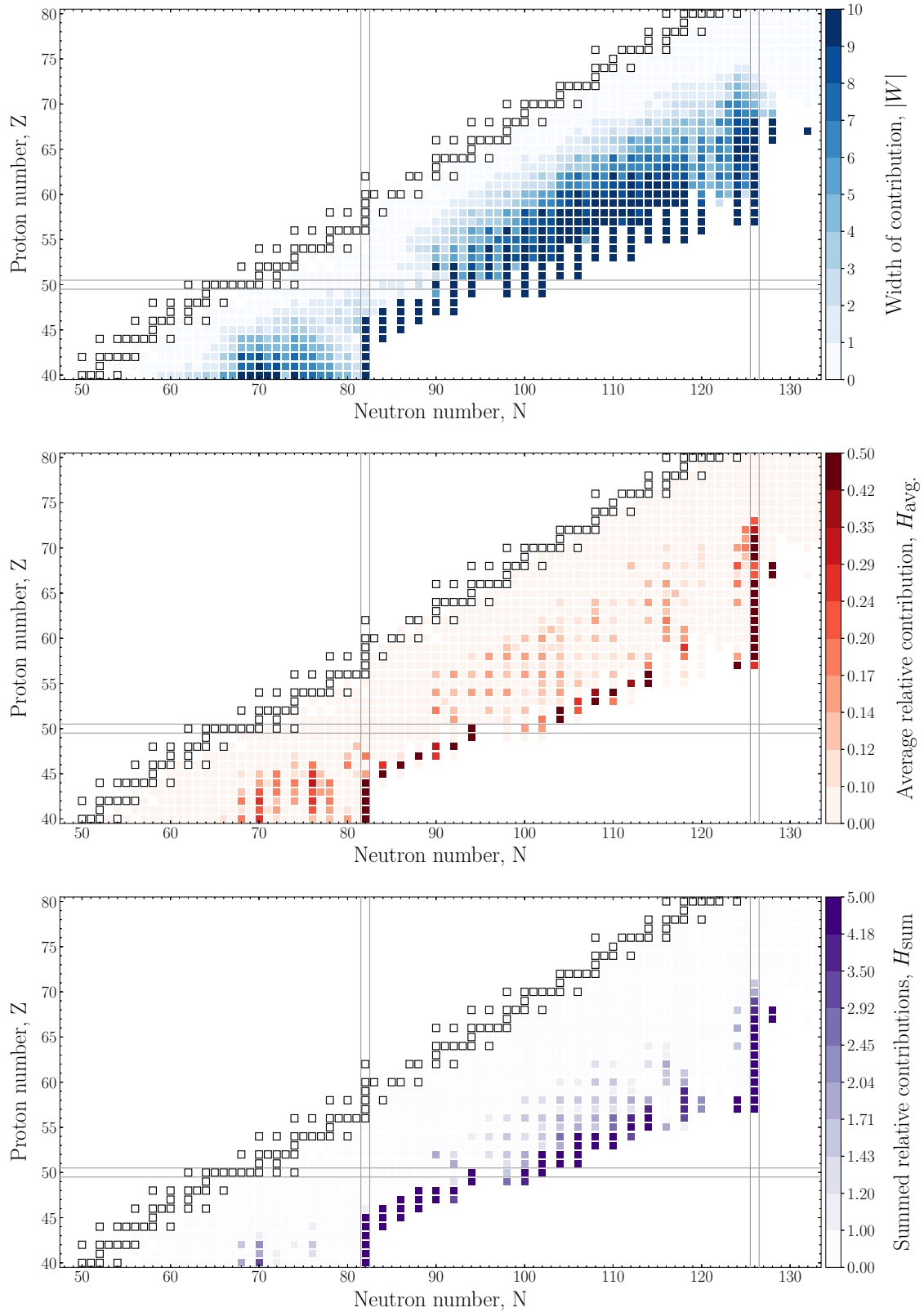
FIG. 13. Average trends in the traced abundances of individual β^- decays for elements $40 < Z < 80$. The top panel shows the width ($|W|$) of the traced abundances, as defined in the text. The middle panel indicates the average relative contribution to total abundances contained within the width ($H_{\text{avg.}}$). The bottom panel gives the the sum of relative contributions to the width (H_{sum}), which may be interpreted as the product of the top and middle panels.

fine the set

$$W = \{A' > A \mid Y_{\text{traced}}(A')/Y(A') > 1\%\}, \quad (13)$$

where A is the mass number of the traced β^- decay parent nucleus. The set W represents the values of A for which the traced abundance represent at least 1% of the final abundance. We refer to the cardinality of the set W as the *width* of the traced pattern. By only considering $A' > A$, we omit any contributions to the final pattern that occur during decay back to stability following the r process. As a result, the width is restricted to contributions that are dynamically involved in the r process.

In the top panel of Fig. 13, we report the width of each of our tracing calculations. For each element, the width is greatest along the r-process path, since the vast majority of abundances of heavier nuclei are produced along this path. Near stability, the width collapses to 0 because all subsequent nucleosynthesis strictly follows a series of β^- decays that preserve mass number A, which is omitted from the set W as we have constructed it. In the intermediate region, there is a smooth transition from larger to smaller widths, with values ranging from 2 to 10 for a relatively large number of nuclei lying away from the r-process path.

It is also instructive to consider the average contribution of a particular β^- decay to the total abundance pattern. We define an additional metric that attempts to provide this insight, defined as

$$H_{\text{avg.}} = \frac{1}{|W|} \sum_{A' \in W} Y_{\text{traced}}(A')/Y(A'), \quad (14)$$

where W is the same as in Eq. (13) and $|W|$ is the width. The value of $H_{\text{avg.}}$ can be understood as the relative contribution of a particular β^- decay, on average, to nuclides contained within the width of the contribution. A large value represents significant contributions to the entirety of the width of the traced pattern, while smaller values correspond to less significant contributions.

Analogous to this metric is the summed relative contributions, given by

$$H_{\text{sum}} = \sum_{A' \in W} Y_{\text{traced}}(A')/Y(A'). \quad (15)$$

Large values in this metric indicate a relatively large width together with significant contributions to overall abundances to the same width.

The values of $H_{\text{avg.}}$ and H_{sum} are shown in the middle and bottom panels of Fig. 13, respectively. As with the widths shown in the top panel, the largest values in each metric lie along the path for the same reasons previously discussed. However, in the intermediate region lying between the r-process path and decay-to-stability nuclides, we can further constrain the list of impactful β^- decays for these conditions. Many of the β^- decays with relatively wide contributions to the abundance pattern have comparatively weak contributions, less than 10%, and may reasonably be considered less important in determining the final abundances overall.

As can be observed in the bottom panel, β^- decay for nuclides nearer the r-process path have sufficiently wide contributions affecting a larger region of the abundance pattern.

For nuclides in the intermediate region but nearer stability, there can be still significant contributions, but these contributions are focused on more constrained regions of the abundance pattern, as they have a significant value for $H_{\text{avg.}}$ but smaller values for the width and, consequently, H_{sum}.

Clearly, β^- decay rates along the r-process path dominate all three of the metrics considered in this section. However, by applying the nucleosynthesis tracing framework, it becomes clear that a large number of β^- decay properties for less neutron-rich nuclides also influence nucleosynthesis in r-process environments.

As a final caution, we point out that these results strongly depend on the astrophysical conditions and the theoretical nuclear models used to supplement available experimental data. Changes to either are liable to affect the r-process path (by adjusting the $(n, \gamma) \rightleftharpoons (\gamma, n)$ equilibrium and point of freeze-out) or the onset of fission recycling, in addition to other possible complications. We propose here only the method by which more robust analyses may proceed in future works. However, we do anticipate the general result to hold; namely, β^- decay rates of many nuclides less neutron-rich than the r-process path are still important in determining nucleosynthesis. We emphasize the importance of future experiments that measure the β^- decay rates (or other properties, such as nuclear masses) for these nuclides, even if the most neutron-rich nuclei remain out of reach for the foreseeable future.

V. CONCLUSION

The most complex examples of nucleosynthesis involve thousands of nuclear species connected by many tens of thousands of nuclear transmutation processes. Owing partly to this complexity, as well as to the generally dynamic and nonlinear nature of nucleosynthesis, it is often difficult to study subsets of nuclear properties in isolation from a nucleosynthetic system as a whole. In this work, we develop our nucleosynthesis tracing framework, which may be applied to partly address this problem.

Beginning with the system of coupled differential equations constituting a standard nuclear reaction network, we frame our tracing framework as the separation of nuclear abundances into two populations, those of *traced* and *untraced* abundances. Furthermore, we allow each transmutation process in a network calculation to be categorized by the way it maps reactants and products between the traced and untraced populations. Within this schema, we derive an additional set of differential equations that model the evolution of the traced abundances. These additional equations are coupled to those of the standard network; when solved together, one obtains a quantitative description of how products from specific nuclear transmutation processes participate in all subsequent nucleosynthesis.

We implement our tracing framework into a new version of our PRISM reaction network, PRISM$^{\text{tr}}$, and comment on several details regarding this implementation. Notably, the tracing network equations are structurally similar to those of a standard reaction network; therefore, numerical techniques commonly used to solve the standard set of network equations

are expected to be equally well suited for solving the tracing network equations.

In order to demonstrate some of the nucleosynthesis analyses enabled by our tracing framework, we perform tracing network calculations using PRISM^{tr} to study fission and β^- decay as they occur in the r process of nucleosynthesis.

Our application of tracing to distinct fission channels can quantify the influence of each channel on forming the final abundance pattern, with qualitative results consistent with investigations of fission in the r process found in the literature. These same calculations offer insight into the extent of fission recycling in an r-process simulation—in particular, they allow for a quantitative distinction between *complete* and *incomplete* fission recycling in the r process that complements existing definitions that compare the abundance of heavy nuclei before and after nucleosynthesis.

When the tracing framework is applied to individual fission reactions and/or decays, we find the fission of a relatively small number of nuclear species along the r-process path drives fission recycling. The fission yields of these nuclei have limited impact on the final abundance pattern since the fission products undergo subsequent neutron captures and are redistributed throughout the network. The shape of the final abundance pattern is instead determined by the product yields of the many nuclear species that fission as the r-process path moves back to stability upon neutron exhaustion. Thus, average trends in fission yields for a large number of nuclei are needed to characterize r-process nucleosynthesis.

Additionally, we apply nucleosynthesis tracing to perform a comprehensive examination of the β^- decay of nuclei with atomic number $40 \leqslant Z \leqslant 80$. We quantify the relative contribution of each β^- decay to r-process nucleosynthesis in neutron star merger wind-like conditions, and we define several metrics that may be useful for characterizing the nature of these contributions.

Finally, we strongly emphasize that our fission and β^- decay results depend on the astrophysical conditions and underlying nuclear models used for this study; a thorough investigation of these dependencies, together with a more comprehensive examination of the numerous and varied nuclear properties entering into r-process nucleosynthesis calculations, is intended for future work.

While we limit the present work to r-process applications, we note that our tracing framework—as we have presented it—is in no way limited to r-process nucleosynthesis, and it may be readily applied to any process for which nuclear reaction networks are appropriate. Indeed, the defining principles of our tracing framework can be naturally adapted to applications outside of nucleosynthesis entirely, e.g., chemical reaction networks.

APPENDIX: SOME COMMENTS ON OUR REACTION NETWORK FORMALISM

The notation we adopt in our construction of the nuclear reaction network equations was chosen to simplify the expressions used in the derivation and statement of the tracing network equations. However, this notation differs from more commonly adopted forms, such as that used in Ref. [19]. Here, we relate our notation to this more common version.

Beginning with Eq. (12) from Ref. [19], the time derivative $\dot{Y}_i$ of each nuclear abundance Y_i is given by

$$\dot{Y}_i = \sum_j \mathcal{N}_j^i \lambda_j Y_j + \sum_{j,k} \mathcal{N}_{j,k}^i \rho N_A \langle j, k \rangle Y_j Y_k$$
$$+ \sum_{j,k,l} \mathcal{N}_{j,k,l}^i \rho^2 N_A^2 \langle j, k, l \rangle Y_j Y_k Y_l, \quad (A1)$$

where each sum is taken over the one-, two-, and three-body reactions in which species i is either created or destroyed. Here, λ_j is a decay rate for species j, ρ is the density, N_A is Avogadro's number, $\langle j, k \rangle$ is the thermal reaction cross section for a reaction between species j and k, and $\langle j, k, l \rangle$ is the thermal cross section for a reaction between species j, k, and l. The $\mathcal{N}_j^i$, $\mathcal{N}_{j,k}^i$, and $\mathcal{N}_{j,k,l}^i$ are numerical factors that correctly count the number of species consumed or produced in each reaction, defined as

$$\mathcal{N}_j^i = N_i,$$
$$\mathcal{N}_{j,k}^i = N_i \Big/ \prod_{m=1}^{n_m} |N_{j_m}|!, \text{ and}$$
$$\mathcal{N}_{j,k,l}^i = N_i \Big/ \prod_{m=1}^{n_m} |N_{j_m}|!, \quad (A2)$$

with N_i giving the number of species i produced (positive) or consumed (negative) by a reaction or decay, and the product in the denominator run over all species consumed by a reaction and corrects for overcounting a reaction involving identical reactants.

In relation to the terminology and notation we use in Sec. II, each term in Eq. (A1) corresponds to a unique process, p, in a network. The processes are grouped into one-, two-, and three-body processes in the first, second, and third sums, respectively. In the case of one-body process, then, we have the associations

(1) $\Lambda_p = \lambda_j$,
(2) $\alpha_p(i) = 1$ if i is a reactant of p and 0 otherwise, and

(3) $\beta_p(i) = |N_i|$ if i is a product of p and 0 otherwise.

For two-body processes, the associations are given by

(1) $\Lambda_p = \rho N_A \langle j, k \rangle \frac{\mathcal{N}^i_{j,k}}{N_i}$,

(2) $\alpha_p(i) = |N_i|$ if i is a reactant of p and 0 otherwise, and

(3) $\beta_p(i) = |N_i|$ if i is a product of p and 0 otherwise.

Finally, for three-body processes, we have

(1) $\Lambda_p = \rho^2 N_A^2 \langle j, k, l \rangle \frac{\mathcal{N}^i_{j,k,l}}{N_i}$,

(2) $\alpha_p(i) = |N_i|$ if i is a reactant of p and 0 otherwise, and

(3) $\beta_p(i) = |N_i|$ if i is a product of p and 0 otherwise.

In all cases, the sets $\mathcal{R}_p$ and $\mathcal{P}_p$ simply collect the reactants and products of the process p, which we use to make explicit the limits of the summations and products used in Eq. (1).

By writing the one-, two-, and three-body terms separately, collecting the positive and negative terms of each into a common summation, and performing the substitutions defined above, Eq. (1) can be rewritten as Eq. (A1).

[1] E. M. Burbidge, G. R. Burbidge, W. A. Fowler, and F. Hoyle, Synthesis of the elements in stars, Rev. Mod. Phys. **29**, 547 (1957).

[2] G. Wallerstein, I. Iben, Jr., P. Parker, A. M. Boesgaard, G. M. Hale, A. E. Champagne, C. A. Barnes, F. Käppeler, V. V. Smith, R. D. Hoffman, F. X. Timmes, C. Sneden, R. N. Boyd, B. S. Meyer, and D. L. Lambert, Synthesis of the elements in stars: Forty years of progress, Rev. Mod. Phys. **69**, 995 (1997).

[3] C. A. Bertulani and A. Gade, Nuclear astrophysics with radioactive beams, Phys. Rep. **485**, 195 (2010).

[4] T. Rauscher, The path to improved reaction rates for astrophysics, Int. J. Mod. Phys. E **20**, 1071 (2011).

[5] C. J. Horowitz, A. Arcones, B. Côté, I. Dillmann, W. Nazarewicz, I. U. Roederer, H. Schatz, A. Aprahamian, D. Atanasov, A. Bauswein, T. C. Beers, J. Bliss, M. Brodeur, J. A. Clark, A. Frebel, F. Foucart, C. J. Hansen, O. Just, A. Kankainen, G. C. McLaughlin *et al.*, r-process nucleosynthesis: Connecting rare-isotope beam facilities with the cosmos, J. Phys. G: Nucl. Phys. **46**, 083001 (2019).

[6] T. Kajino, W. Aoki, A. B. Balantekin, R. Diehl, M. A. Famiano, and G. J. Mathews, Current status of r-process nucleosynthesis, Prog. Part. Nucl. Phys. **107**, 109 (2019).

[7] J. J. Cowan, C. Sneden, J. E. Lawler, A. Aprahamian, M. Wiescher, K. Langanke, G. Martínez-Pinedo, and F.-K. Thielemann, Origin of the heaviest elements: The rapid neutron-capture process, Rev. Mod. Phys. **93**, 015002 (2021).

[8] H. Schatz, A. Aprahamian, J. Goerres, M. Wiescher, T. Rauscher, J. F. Rembges, F. K. Thielemann, B. Pfeiffer, P. Moeller, K. L. Kratz, H. Herndl, B. A. Brown, and H. Rebel, rp-process nucleosynthesis at extreme temperature and density conditions, Phys. Rep. **294**, 167 (1998).

[9] C. Iliadis, A. Champagne, J. José, S. Starrfield, and P. Tupper, The effects of thermonuclear reaction-rate variations on nova nucleosynthesis: A sensitivity study, Astrophys. J. Suppl. Ser. **142**, 105 (2002).

[10] M. R. Mumpower, R. Surman, G. C. McLaughlin, and A. Aprahamian, The impact of individual nuclear properties on r-process nucleosynthesis, Prog. Part. Nucl. Phys. **86**, 86 (2016).

[11] R. Surman, M. Mumpower, and A. Aprahamian, Uncorrelated nuclear mass uncertainties and r-process abundance predictions, Acta Phys. Pol. B **47**, 673 (2016).

[12] D. Martin, A. Arcones, W. Nazarewicz, and E. Olsen, Impact of Nuclear Mass Uncertainties on the r Process, Phys. Rev. Lett. **116**, 121101 (2016).

[13] J. Bliss, A. Arcones, F. Montes, and J. Pereira, Impact of (α, n) reactions on weak r-process in neutrino-driven winds, J. Phys. G: Nucl. Phys. **44**, 054003 (2017).

[14] P. Denissenkov, G. Perdikakis, F. Herwig, H. Schatz, C. Ritter, M. Pignatari, S. Jones, S. Nikas, and A. Spyrou, The impact of (n, γ) reaction rate uncertainties of unstable isotopes near $N = 50$ on the i-process nucleosynthesis in He-shell flash white dwarfs, J. Phys. G: Nucl. Phys. **45**, 055203 (2018).

[15] T. M. Sprouse, R. Navarro Perez, R. Surman, M. R. Mumpower, G. C. McLaughlin, and N. Schunck, Propagation of statistical uncertainties of Skyrme mass models to simulations of r-process nucleosynthesis, Phys. Rev. C **101**, 055803 (2020).

[16] S. Wanajo, Cold r-process in neutrino-driven winds, Astrophys. J. Lett. **666**, L77 (2007).

[17] M. R. Mumpower, T. Kawano, T. M. Sprouse, N. Vassh, E. M. Holmbeck, R. Surman, and P. Möller, β-delayed fission in r-process nucleosynthesis, Astrophys. J. **869**, 14 (2018).

[18] N. Vassh, R. Vogt, R. Surman, J. Randrup, T. M. Sprouse, M. R. Mumpower, P. Jaffke, D. Shaw, E. M. Holmbeck, Y. Zhu, and G. C. McLaughlin, Using excitation-energy dependent fission yields to identify key fissioning nuclei in r-process nucleosynthesis, J. Phys. G: Nucl. Phys. **46**, 065202 (2019).

[19] W. R. Hix and F. K. Thielemann, Computational methods for nucleosynthesis and nuclear energy generation, J. Comput. Appl. Math. **109**, 321 (1999).

[20] W. D. Arnett and J. W. Truran, Carbon-burning nucleosynthesis at constant temperature, Astrophys. J. **157**, 339 (1969).

[21] S. E. Woosley, W. D. Arnett, and D. D. Clayton, The explosive burning of oxygen and silicon, Astrophys. J. Suppl. Ser. **26**, 231 (1973).

[22] W. R. Hix and B. S. Meyer, Thermonuclear kinetics in astrophysics, Nucl. Phys. A **777**, 188 (2006).

[23] J. Lippuner and L. F. Roberts, SkyNet: A modular nuclear reaction network library, Astrophys. J. Suppl. Ser. **233**, 18 (2017).

[24] F. X. Timmes, Integration of nuclear reaction networks for stellar hydrodynamics, Astrophys. J. Suppl. Ser. **124**, 241 (1999).

[25] M. Guidry, Algebraic stabilization of explicit numerical integration for extremely stiff reaction networks, J. Comput. Phys. **231**, 5266 (2012).

[26] M. W. Guidry, R. Budiardja, E. Feger, J. J. Billings, W. R. Hix, O. E. B. Messer, K. J. Roche, E. McMahon, and M. He, Explicit integration of extremely stiff reaction networks: Asymptotic methods, Comp. Sci. Disc. **6**, 015001 (2013).

[27] M. W. Guidry and J. A. Harris, Explicit integration of extremely stiff reaction networks: Quasi-steady-state methods, Comp. Sci. Disc. **6**, 015002 (2013).

[28] M. W. Guidry, J. J. Billings, and W. R. Hix, Explicit integration of extremely stiff reaction networks: partial equilibrium methods, Comp. Sci. Disc. **6**, 015003 (2013).

[29] B. Brock, A. Belt, J. J. Billings, and M. Guidry, Explicit in-

tegration with GPU acceleration for large kinetic networks, J. Comput. Phys. **302**, 591 (2015).

[30] M. R. Mumpower, T. Kawano, J. L. Ullmann, M. Krtička, and T. M. Sprouse, Estimation of $M1$ scissors mode strength for deformed nuclei in the medium- to heavy-mass region by statistical Hauser-Feshbach model calculations, Phys. Rev. C **96**, 024612 (2017).

[31] Y. Zhu, R. T. Wollaeger, N. Vassh, R. Surman, T. M. Sprouse, M. R. Mumpower, P. Möller, G. C. McLaughlin, O. Korobkin, T. Kawano, P. J. Jaffke, E. M. Holmbeck, C. L. Fryer, W. P. Even, A. J. Couture, and J. Barnes, Californium-254 and Kilonova light curves, Astrophys. J. Lett. **863**, L23 (2018).

[32] R. H. Cyburt, A. M. Amthor, R. Ferguson, Z. Meisel, K. Smith, S. Warren, A. Heger, R. D. Hoffman, T. Rauscher, A. Sakharuk, H. Schatz, F. K. Thielemann, and M. Wiescher, The JINA REACLIB database: Its recent updates and impact on type-I x-ray bursts, Astrophys. J. Suppl. **189**, 240 (2010).

[33] M. R. Mumpower, T. Kawano, and P. Möller, Neutron-γ competition for β-delayed neutron emission, Phys. Rev. C **94**, 064317 (2016).

[34] P. Möller, M. R. Mumpower, T. Kawano, and W. D. Myers, Nuclear properties for astrophysical and radioactive-ion-beam applications (II), At. Data Nucl. Data Tables **125**, 1 (2019).

[35] M. Wang, G. Audi, F. G. Kondev, W. J. Huang, S. Naimi, and X. Xu, The AME2016 atomic mass evaluation (II): Tables, graphs, and references, Chin. Phys. C **41**, 030003 (2017).

[36] P. Möller, W. D. Myers, H. Sagawa, and S. Yoshida, Phys. Rev. Lett. **108**, 052501 (2012).

[37] T. Kawano, R. Capote, S. Hilaire, and P. C. Huu-Tai, Phys. Rev. C **94**, 014612 (2016).

[38] M. R. Mumpower, P. Jaffke, M. Verriere, and J. Randrup, Primary fission fragment mass yields across the chart of nuclides, Phys. Rev. C **101**, 054607 (2020).

[39] G. Audi, F. G. Kondev, M. Wang, W. J. Huang, and S. Naimi, The nubase2016 evaluation of nuclear properties, Chin. Phys. C **41**, 030001 (2017).

[40] N. R. Council, D. E. P. Sciences, B. P. Astronomy, and C. P. Universe, *Connecting Quarks with the Cosmos: Eleven Science Questions for the New Century* (National Academies Press, Washington, D.C., 2003).

[41] T. C. A. O. N. Physics, B. P. Astronomy, D. E. P. Sciences, and N. R. Council, *Nuclear Physics: Exploring the Heart of Matter* (National Academies Press, Washington, D.C., 2013).

[42] B. P. Abbott, R. Abbott, T. D. Abbott, F. Acernese, K. Ackley, C. Adams, T. Adams, P. Addesso, R. X. Adhikari, V. B. Adya, et al., Gw170817: Observation of Gravitational Waves from a Binary Neutron Star Inspiral, Phys. Rev. Lett. **119**, 161101 (2017).

[43] B. P. Abbott, R. Abbott, T. D. Abbott, F. Acernese, K. Ackley, C. Adams, T. Adams, P. Addesso, R. X. Adhikari, V. B. Adya, et al., Multi-messenger observations of a binary neutron star merger, Astrophys. J. Lett. **848**, L12 (2017).

[44] P. S. Cowperthwaite, E. Berger, V. A. Villar, B. D. Metzger, M. Nicholl, R. Chornock, P. K. Blanchard, W. Fong, R. Margutti, M. Soares-Santos, et al., The electromagnetic counterpart of the binary neutron star merger LIGO/VIRGO GW170817. II. UV, optical, and near-infrared light curves and comparison to kilonova models, Astrophys. J. Lett. **848**, L17 (2017).

[45] J. Beun, G. C. McLaughlin, R. Surman, and W. R. Hix, Fission cycling in a supernova r process, Phys. Rev. C **77**, 035804 (2008).

[46] O. Korobkin, S. Rosswog, A. Arcones, and C. Winteler, On the astrophysical robustness of the neutron star merger r-process, Mon. Not. R. Astron. Soc. **426**, 1940 (2012).

[47] S. Goriely, The fundamental role of fission during r-process nucleosynthesis in neutron star mergers, Eur. Phys. J. A **51**, 22 (2015).

[48] M. Eichler, A. Arcones, A. Kelic, O. Korobkin, K. Langanke, T. Marketin, G. Martinez-Pinedo, I. Panov, T. Rauscher, S. Rosswog, C. Winteler, N. T. Zinner, and F. K. Thielemann, The role of fission in neutron star mergers and its impact on the r-process peaks, Astrophys. J. **808**, 30 (2015).

[49] N. Vassh, M. R. Mumpower, G. C. McLaughlin, T. M. Sprouse, and R. Surman, Co-production of light and heavy r-process elements via fission deposition, Astrophys. J. **896**, 28 (2020).

[50] K.-H. Schmidt and B. Jurado, Review on the progress in nuclear fission—experimental methods and theoretical descriptions, Rep. Prog. Phys. **81**, 106301 (2018).

[51] S. A. Giuliani, G. Martínez-Pinedo, and L. M. Robledo, Fission properties of superheavy nuclei for r-process calculations, Phys. Rev. C **97**, 034323 (2018).

[52] J. F. Lemaître, S. Goriely, S. Hilaire, and N. Dubray, Microscopic description of the fission path with the Gogny interaction, Phys. Rev. C **98**, 024623 (2018).

[53] J. F. Lemaître, S. Goriely, S. Hilaire, and J. L. Sida, Fully microscopic scission-point model to predict fission fragment observables, Phys. Rev. C **99**, 034612 (2019).

[54] J. Sadhukhan, S. A. Giuliani, Z. Matheson, and W. Nazarewicz, Efficient method for estimation of fission fragment yields of r-process nuclei, Phys. Rev. C **101**, 065803 (2020).

[55] T. Piran, E. Nakar, and S. Rosswog, The electromagnetic signals of compact binary mergers, Mon. Not. R. Astron. Soc. **430**, 2121 (2013).

[56] S. Rosswog, T. Piran, and E. Nakar, The multimessenger picture of compact object encounters: Binary mergers versus dynamical collisions, Mon. Not. R. Astron. Soc. **430**, 2585 (2013).

[57] I. Petermann, A. Arcones, A. Kelić, K. Langanke, G. Martínez-Pinedo, K. H. Schmidt, W. R. Hix, I. Panov, T. Rauscher, F. K. Thielemann, and N. Zinner, Towards r-process nucleosynthesis calculations with complete nuclear physics input, in *Nuclei in the Cosmos (NIC X)* (Sissa Medialab srl, Trieste, Italy, 2008), p. E143.

[58] J. Lippuner and L. F. Roberts, r-process lanthanide production and heating rates in kilonovae, Astrophys. J. **815**, 82 (2015).

[59] J. Erler, N. Birge, M. Kortelainen, W. Nazarewicz, E. Olsen, A. M. Perhac, and M. Stoitsov, The limits of the nuclear landscape, Nature (London) **486**, 509 (2012).

[60] J. D. McDonnell, N. Schunck, D. Higdon, J. Sarich, S. M. Wild, and W. Nazarewicz, Uncertainty Quantification for Nuclear Density Functional Theory and Information Content of New Measurements, Phys. Rev. Lett. **114**, 122501 (2015).

[61] L. Neufcourt, Y. Cao, S. A. Giuliani, W. Nazarewicz, E. Olsen, and O. B. Tarasov, Quantified limits of the nuclear landscape, Phys. Rev. C **101**, 044307 (2020).

[62] N. D. Scielzo, G. Li, M. G. Sternberg, G. Savard, P. F. Bertone, F. Buchinger, S. Caldwell, J. A. Clark, J. Crawford, C. M. Deibel, J. Fallis, J. P. Greene, S. Gulick, A. A. Hecht, D. Lascar, J. K. P. Lee, A. F. Levand, M. Pedretti, R. E. Segel, H. Sharma *et al.*, The β-decay Paul trap: A radiofrequency-quadrupole ion trap for precision β-decay studies, Nucl. Instrum. Methods Phys. Res., Sect. A **681**, 94 (2012).

[63] R. M. Yee, N. D. Scielzo, P. F. Bertone, F. Buchinger, S. Caldwell, J. A. Clark, C. M. Deibel, J. Fallis, J. P. Greene, S. Gulick, D. Lascar, A. F. Levand, G. Li, E. B. Norman, M. Pedretti, G. Savard, R. E. Segel, K. S. Sharma, M. G. Sternberg, J. Van Schelt *et al.*, β-Delayed Neutron Spectroscopy Using Trapped Radioactive Ions, Phys. Rev. Lett. **110**, 092501 (2013).

[64] N. D. Scielzo, R. M. Yee, P. F. Bertone, F. Buchinger, S. A. Caldwell, J. A. Clark, A. Czeszumska, C. M. Deibel, J. P. Greene, S. Gulick, D. Lascar, A. F. Levand, G. Li, E. B. Norman, S. Padgett, M. Pedretti, A. Perez Galvan, G. Savard, R. E. Segel, K. S. Sharma, M. G. Sternberg *et al.*, A novel approach to β-delayed neutron spectroscopy using the β-decay Paul trap, Nucl. Data Sheets **120**, 70 (2014).

[65] B. S. Wang, S. A. Caldwell, N. D. Scielzo, A. Czeszumska, J. A. Clark, G. Savard, A. Aprahamian, M. T. Burkey, C. J. Chiara, J. Harker, A. F. Levand, S. T. Marley, G. E. Morgan, J. M. Munson, E. B. Norman, A. Nystrom, R. Orford, S. W. Padgett, A. Pérez Galván, K. S. Sharma, K. Siegl *et al.*, β-delayed-neutron studies of ^{136,135}Sb and ^{140}I performed with trapped ions, Phys. Rev. C **101**, 025806 (2020).

[66] T. Y. Hirsh, N. Paul, M. Burkey, A. Aprahamian, F. Buchinger, S. Caldwell, J. A. Clark, A. F. Levand, L. L. Ying, S. T. Marley, G. E. Morgan, A. Nystrom, R. Orford, A. P. Galván, J. Rohrer, G. Savard, K. S. Sharma, and K. Siegl, First operation and mass separation with the CARIBU MR-TOF, Nucl. Instrum. Methods Phys. Res., Sect. B **376**, 229 (2016).

[67] R. Orford, N. Vassh, J. A. Clark, G. C. McLaughlin, M. R. Mumpower, G. Savard, R. Surman, A. Aprahamian, F. Buchinger, M. T. Burkey, D. A. Gorelov, T. Y. Hirsh, J. W. Klimes, G. E. Morgan, A. Nystrom, and K. S. Sharma, Precision Mass Measurements of Neutron-Rich Neodymium and Samarium Isotopes and Their Role in Understanding Rare-Earth Peak Formation, Phys. Rev. Lett. **120**, 262702 (2018).

[68] G. Savard, M. Brodeur, J. A. Clark, R. A. Knaack, and A. A. Valverde, The $N = 126$ factory: A new facility to produce very heavy neutron-rich isotopes, Nucl. Instrum. Methods Phys. Res., Sect. B **463**, 258 (2020).

[69] A. Kankainen, J. Hakala, T. Eronen, D. Gorelov, A. Jokinen, V. S. Kolhinen, I. D. Moore, H. Penttilä, S. Rinta-Antila, J. Rissanen, A. Saastamoinen, V. Sonnenschein, and J. Äystö, Isomeric states close to doubly magic ^{132}Sn studied with the double Penning trap JYFLTRAP, Phys. Rev. C **87**, 024307 (2013).

[70] M. Vilen, J. M. Kelly, A. Kankainen, M. Brodeur, A. Aprahamian, L. Canete, T. Eronen, A. Jokinen, T. Kuta, I. D. Moore, M. R. Mumpower, D. A. Nesterenko, H. Penttilä, I. Pohjalainen, W. S. Porter, S. Rinta-Antila, R. Surman, A. Voss, and J. Ńystö, Precision Mass Measurements on Neutron-Rich Rare-Earth Isotopes at JYFLTRAP: Reduced Neutron Pairing and Implications for R-Process Calculations, Phys. Rev. Lett. **120**, 262701 (2018).

[71] D. Lunney *et al.* (ISOLTRAP Collaboration), Extending and refining the nuclear mass surface with ISOLTRAP, J. Phys. G: Nucl. Phys. **44**, 064008 (2017).

[72] D. Lascar, R. Klawitter, C. Babcock, E. Leistenschneider, S. R. Stroberg, B. R. Barquest, A. Finlay, M. Foster, A. T. Gallant, P. Hunt, J. Kelly, B. Kootte, Y. Lan, S. F. Paul, M. L. Phan, M. P. Reiter, B. Schultz, D. Short, J. Simonis, C. Andreoiu *et al.* Precision mass measurements of $^{125–127}$Cd isotopes and isomers approaching the $N = 82$ closed shell, arXiv e-print.

[73] B. Moon, C. B. Moon, P. A. Söderström, A. Odahara, R. Lozeva, B. Hong, F. Browne, H. S. Jung, P. Lee, C. S. Lee, A. Yagi, C. Yuan, S. Nishimura, P. Doornenbal, G. Lorusso, T. Sumikama, H. Watanabe, I. Kojouharov, T. Isobe, H. Baba *et al.*, Nuclear structure and β-decay schemes for Te nuclides beyond $N = 82$, Phys. Rev. C **96**, 044323 (2017).

[74] N. Fukuda, T. Kubo, D. Kameda, N. Inabe, H. Suzuki, Y. Shimizu, H. Takeda, K. Kusaka, Y. Yanagisawa, M. Ohtake, K. Tanaka, K. Yoshida, H. Sato, H. Baba, M. Kurokawa, T. Ohnishi, N. Iwasa, A. Chiba, T. Yamada, E. Ideguchi *et al.*, Identification of new neutron-rich isotopes in the rare-earth region produced by 345 MeV/nucleon ^{238}U, J. Phys. Soc. Jpn. **87**, 014202 (2018).

[75] A. Tolosa-Delgado, J. Agramunt, J. L. Tain, A. Algora, C. Domingo-Pardo, A. I. Morales, B. Rubio, A. Tarifeño-Saldivia, F. Calviño, G. Cortes, N. T. Brewer, B. C. Rasco, K. P. Rykaczewski, D. W. Stracener, J. M. Allmond, R. Grzywacz, R. Yokoyama, M. Singh, T. King, M. Madurga *et al.* (Briken Collaboration), Commissioning of the BRIKEN detector for the measurement of very exotic β-delayed neutron emitters, Nucl. Instrum. Methods Phys. Res., Sect. A **925**, 133 (2019).

[76] H. Stöcker, T. Stöhlker, and C. Sturm, FAIR—Cosmic matter in the laboratory, J. Phys. Conf. Ser. **623**, 012026 (2015).

[77] R. Caballero-Folch, C. Domingo-Pardo, J. Agramunt, A. Algora, F. Ameil, Y. Ayyad, J. Benlliure, M. Bowry, F. Calviño, D. Cano-Ott, G. Cortès, T. Davinson, I. Dillmann, A. Estrade, A. Evdokimov, T. Faestermann, F. Farinon, D. Galaviz, A. R. García, H. Geissel *et al.*, β-decay half-lives and β-delayed neutron emission probabilities for several isotopes of Au, Hg, Tl, Pb, and Bi, beyond $N = 126$, Phys. Rev. C **95**, 064322 (2017).

[78] A. Gottardo, J. J. Valiente-Dobón, G. Benzoni, A. I. Morales, A. Gadea, S. Lunardi, P. Boutachkov, A. M. Bruce, M. Górska, J. Grebosz, S. Pietri, Z. Podolyák, M. Pfützner, P. H. Regan, D. Rudolph, H. Weick, J. A. Núñez, A. Algora, N. Al-Dahan, G. de Angelis *et al.*, New spectroscopic information ^{213,211}Tl: A changing structure beyond the N=126 shell closure, Phys. Rev. C **99**, 054326 (2019).

[79] https://groups.nscl.msu.edu/frib/rates/fribrates.html

[80] M. R. Mumpower, R. Surman, D. L. Fang, M. Beard, P. Möller, T. Kawano, and A. Aprahamian, Impact of individual nuclear masses on r-process abundances, Phys. Rev. C **92**, 035807 (2015).

[81] R. Surman, J. Engel, J. R. Bennett, and B. S. Meyer, Source of the Rare-Earth Element Peak in r-Process Nucleosynthesis, Phys. Rev. Lett. **79**, 1809 (1997).

[82] R. Surman and J. Engel, Changes in r-process abundances at late times, Phys. Rev. C **64**, 035801 (2001).

[83] A. Arcones and G. Martínez-Pinedo, Dynamical r-process studies within the neutrino-driven wind scenario and its sensitivity to the nuclear physics input, Phys. Rev. C **83**, 045809 (2011).

[84] M. R. Mumpower, G. C. McLaughlin, and R. Surman, Formation of the rare-earth peak: Gaining insight into late-time r-process dynamics, Phys. Rev. C **85**, 045801 (2012).

[85] M. Mumpower, J. Cass, G. Passucci, R. Surman, and A. Aprahamian, Sensitivity studies for the main r process: β-decay rates, AIP Adv. **4**, 041009 (2014).